Recurrence quantification analysis of nonlinear dynamical systems

Article · January 2005

CITATIONS
573

READS
5,422

2 authors, including:

Charles L Webber
Loyola University Chicago, Stritch School of Medicine - Health Sciences Division
121 PUBLICATIONS **7,931** CITATIONS

SEE PROFILE

CHAPTER 2

Recurrence Quantification Analysis of Nonlinear Dynamical Systems

Charles L. Webber, Jr.

Department of Physiology
Loyola University Medical Center
Maywood, Illinois 60153-3304
U. S. A.
E-mail: cwebber@lumc.edu

Joseph P. Zbilut

Department of Molecular Biophysics and Physiology
Rush University Medical Center
Chicago, IL 60612-3839
U. S. A.
E-mail: jzbilut@rush.edu

RECURRENCES IN NATURE

Comprehension of the physical world depends upon observation, measurement, analysis, and, if possible, prediction of patterns expressed ubiquitously in nature. Linear or near-linear systems possess a regularity and simplicity that are readily amenable to scientific investigations. Yet numerous other systems, especially those in the animate realm, possess complexities that are at best non-linear and non-predictable. Common ground between living and non-living systems resides in their shared property of recurrence. That is, within the dynamical signals expressed by living and non-living signals are stretches, short or long, of repeating patterns. Actually, recurrence properties are taken advantage of in signal compression techniques (Wyner, Ziv, & Wyner, 1998)—one billion sine waves at a constant frequency will perfectly collapse to a fraction of one sine cycle with loss of no information. As signals grow in complexity, however, recurrences become rarer, and efficient compressibility is resisted. For so-called random systems such as radioactive decay, recurrences occur theoretically by chance alone. But the lesson is clear: Insofar as natural patterns are found in all dynamical systems, the degree to which those systems exhibit recurrent patterns speaks volumes regarding their underlying dynamics. And, on reflection, it should be appreciated that the entire scientific enterprise is based upon the concept of recurrence: To be accepted as valid, experimental results must be repeatable in the hands of the primary investigator and verifiable by independent laboratories.

Patterns of recurrence in nature necessarily have mathematical underpinnings (Eckmann, Kamphorst, & Ruelle, 1987) which will

readily become apparent in the sections that follow. Although recurrence quantification analysis (RQA) is scantly a decade old (Zbilut & Webber, 1992; Webber & Zbilut, 1994), the concept of recurrence in mathematics has a much longer history (Feller, 1950; Kac, 1959). However, any appreciation of nonlinear dynamics and associated terms the reader brings to the table (fractals, attractors, non-stationarity, singularities, etc.) will greatly facilitate the comprehension of recurrence analysis (see Glass & Mackey, 1988; Bassingthwaighte, Liebovitch, & West, 1994; Kaplan & Glass, 1995). Indeed, our primary goal in this chapter is to provide clear details regarding the proper implementation of one nonlinear technique, RQA, in the assessment or diagnosis of complex dynamical systems. Using carefully selected examples pertinent to the field of psychology and parallel disciplines, we will build a case for the fundamentals of RQA, its derivation, and its utility. Patience is required of the learner, for there are no short cuts to RQA strategies; proper implementations are application-specific. A mathematical framework is constructed to give quantitative legitimacy to RQA, but for those unfamiliar with mathematical notation, an Appendix is provided with discrete numerical examples (Webber, 2004).

The up and down motions of sea waves originally inspired Joseph Fourier to characterize signals in terms of their frequency-domain features (e.g., cycles per sec); that technique now bears his name (Grafakos, 2003). Likewise, for our recurrence purposes, consider a system of literal waves on the sea as measured from buoy instrumentation and plotted in Figure 2.1A. During the 9.4 days of 226 hourly measurements the wave heights rise and fall in a nonlinear,

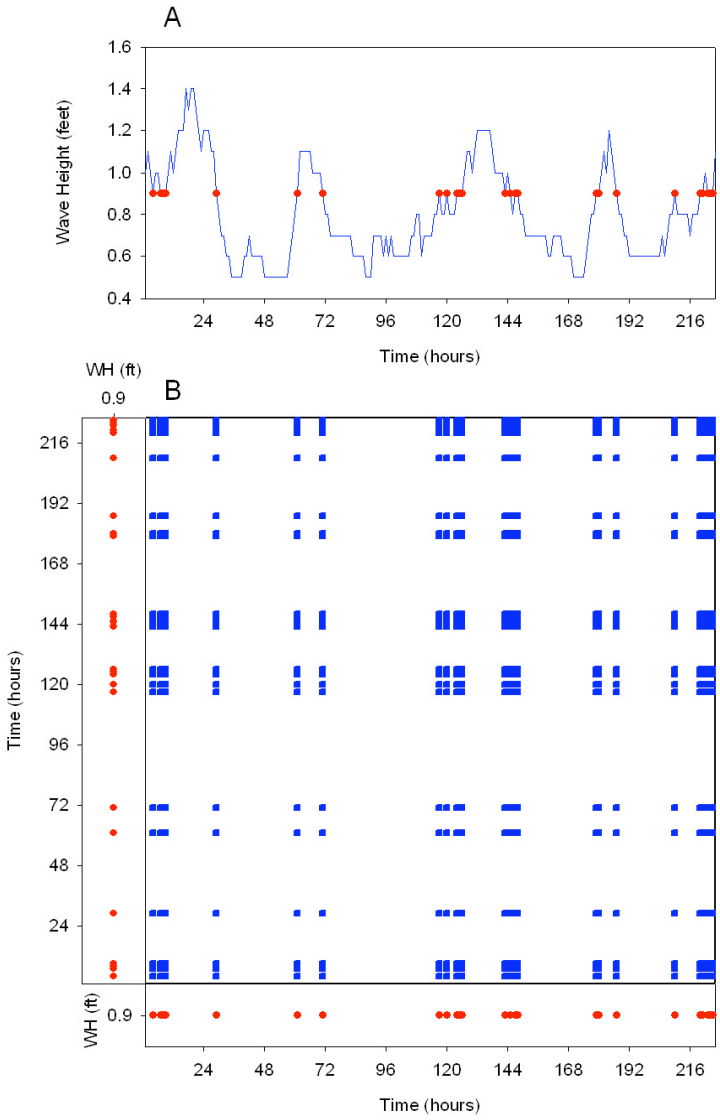

Figure 2.1. (A) Wave height measurements recorded hourly for 226 hours from buoy instrumentation located 33 nautical miles south of Islip, LI, NY (National Data Buoy Center Station 44025). Wave heights are expressed in feet to the nearest 0.1 ft from hour 14, July 10 through hour 23, July 19, 2002. Dots are placed on all waves having identical heights of exactly 0.9 ft that occur at 25 aperiodic points in time (hours: 4, 7-9, 29, 61, 71, 117, 120, 124-126, 143, 145, 147-148, 179-180, 187, 210, 220-221, 223-225). These wave data are owned by the NSW Department of Land and Water Conservation (DLWC) as collected and provided by the Manly Hydraulic Laboratory (MHL), Sydney, Australia. Time series data from data file *BOUY* (n=226 points). (B) Matrix plot of identical wave heights at 0.9 ft. The same time series of 25 aperiodic time points is aligned along both horizontal and vertical time axes, and intersecting pixels are darkened to map out recurrence matches at 0.9 ft wave heights only. All other wave heights are excluded from the matrix. Recurrence data computed from data file *BUOY9* using program *RQD.EXE*. RQA parameters: P_1-P_{last} = 1-226; RANDSEQ = n; NORM = max norm; DELAY = 1; EMBED = 1; RESCALE = absolute; RADUS = 0; COLORBND = 1; LINE = 2.

aperiodic fashion over different time scales (long-periods, large amplitudes; short-periods, small amplitudes). To capture the fundamental notion of recurrence, a dot is placed on every wave of the time series that is exactly 0.9 ft in height. As illustrated, this forms an imaginary line of horizontal dots cutting through the waves at 25 specific time points. That is, each of these waves is exactly recurrent (same height) with one another at certain instances in time that are non-periodic. To graphically represent the recurrent structuring of the data matrix at 0.9 ft height only, the time-positions of these waves are plotted against each other in Figure 2.1B. All other wave heights are excluded.

To get a more accurate picture, however, it is necessary to include waves of all possible heights. Because the waves range in height from 0.5 to 1.4 ft with a measurement resolution of 0.1 ft, there are necessarily 10 different possible wave heights. The recurrence plot of Figure 2.2A shows the distribution of recurrent points (darkened pixels) for all waves of exactly the same height, including low-, medium-, and high-amplitude waves. For the sea wave data it can be seen that the recurrence plot forms a delicate, lace-like pattern of recurrent points. By necessity, there is a long diagonal line (wave heights always self-match), the plot is symmetrical across that diagonal (if height of wave i matches height of wave j, then the height of wave j matches height of wave i), and the recurrence plot is 2-dimensional.

What happens if we relax the constraint that wave heights must be exactly the same before registering them as recurrent? For example, if we let sea waves within 0.2 ft of each other be considered recurrent, a 1.0 ft wave would recur with other waves ranging in height

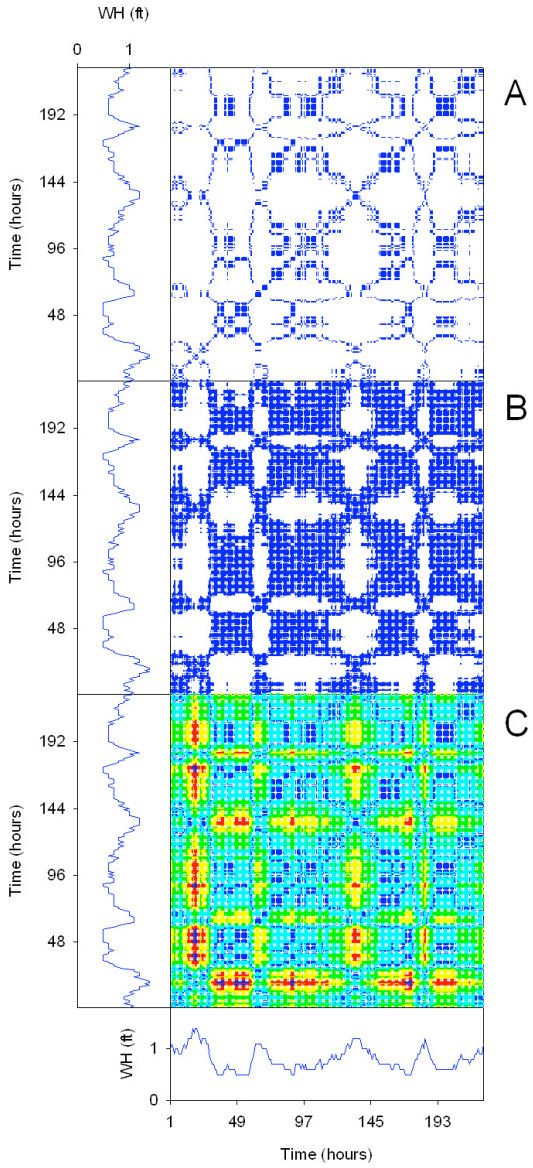

Figure 2.2. Recurrence plots of wave height data for different radius (RADIUS) settings and computed recurrence densities (%REC). (A) Exact recurrences (RADIUS = 0.0 ft; %REC = 13.479%). (B) Approximate recurrences (RADIUS = 0.2 ft; %REC = 54.938%). (C) Saturated recurrences (RADIUS = 0.9 ft, %REC = 100.000%). Like color-contour maps, the recurrence plot in C is color-coded in 0.2 ft increments of RADIUS: blue (0.0-0.2 ft); cyan (0.2-0.4 ft); green (0.4-0.6 ft); yellow (0.6-0.8 ft); red (0.8-0.9 ft). Time series of wave height data (WH, feet versus hours) align along the horizontal and vertical axes of each recurrence plot (time calibration of hour 1 through hour 226). Recurrence data computed from file *BUOY* using program *RQD.EXE*. RQA parameters: P_1-P_{last} = 1-226; RANDSEQ = n; NORM = max norm; DELAY = 1; EMBED = 1; RESCALE = absolute; RADIUS = 0.0 (A), 0.2 (B) or 1.0 (C); COLORBND = 1 (A and B) or 0.2 (C); LINE = 2.

from 0.8 to 1.2 ft. Therefore, applying this rule to all points in the time series should result in the recruitment of more recurrent points. Indeed this is the case, as demonstrated in the recurrence plot of Figure 2.2B. The density of recurrences is decidedly higher, and the lace-like quality of the former plot is replaced by broader areas of approximate recurrences. Carrying this relaxation rule to its limit, what would the recurrence plot look like if all waves were recurrent with one another? This is easily done for the present example by defining two time-points recurrent if they are within 0.9 ft in height. The 0.9 ft limit comes from the difference between the largest wave (1.4 ft) and the smallest wave (0.4 ft). In this case, we would correctly expect every pixel in the recurrence plot to be selected, creating one huge dark square with loss of all subtle details (not shown). Discriminating details of distances can be retrieved, however, by color-coding the differences in wave heights according to a simple coloring scheme as illustrated in Figure 2.2C. All we need to do is change the assigned color in 0.2 ft increments, constructing a color-contour map of wave heights. Actually, this type of coloring is not unlike any contour mapping using different colors to designate various elevations above or below sea level. It is very instructive to make mental correlations between the wave height data (time series along horizontal and vertical axes) and the attendant recurrence plots.

RECURRENCE PLOTS

With this simple introduction to recurrence plots, it is now necessary to become more mathematical. Published numerical examples (Webber, 2004) are reiterated in the Appendix to assist in the

learning of these important details. As will be carefully shown, the recurrence plot is nothing more (or less) than the visualization of a square recurrence matrix (RM) of distance elements within a cutoff limit. We will work up to the definition of seven recurrence parameters (user-adjustable constants) which control the distances within the matrix, their rescaling, and recurrence plot texture. To do this, we will introduce the straightforward ECG signal recorded from a human volunteer as plotted in Figure 2.3A. We could easily generate a recurrence plot of this signal like was done for the sea wave data, identifying as recurrent those time points with identical or similar voltages. But to do so would only be the first-dimensional approach to the problem (represented in a 2-dimensional recurrence plot); as we describe in the following paragraphs, such a 1-dimensional approach may not suffice.

Consider the ECG signal in its one-dimensaional representation of voltage as a function of time (Figure 2.3A). Does not this signal actually "live" in higher dimensions? Of course it does. Since the ECG derives from summed cardiac potentials that move simultaneously in three dimensions (frontal, saggital, and horizontal orthogonal planes), the 1- and 2-dimensional representations are mere projections of the signal to lower dimensions. To accurately represent the ECG in three dimensions it would be necessary to simultaneously record electrical potentials in three orthogonal planes from the subject. But here is where things get very interesting. About a quarter century ago Takens (1981), elaborating upon key conceptual ideas of Ruelle, introduced his theorem of higher-dimensional reconstruction by the method of time delays. What this theorem states is that the topological features of any

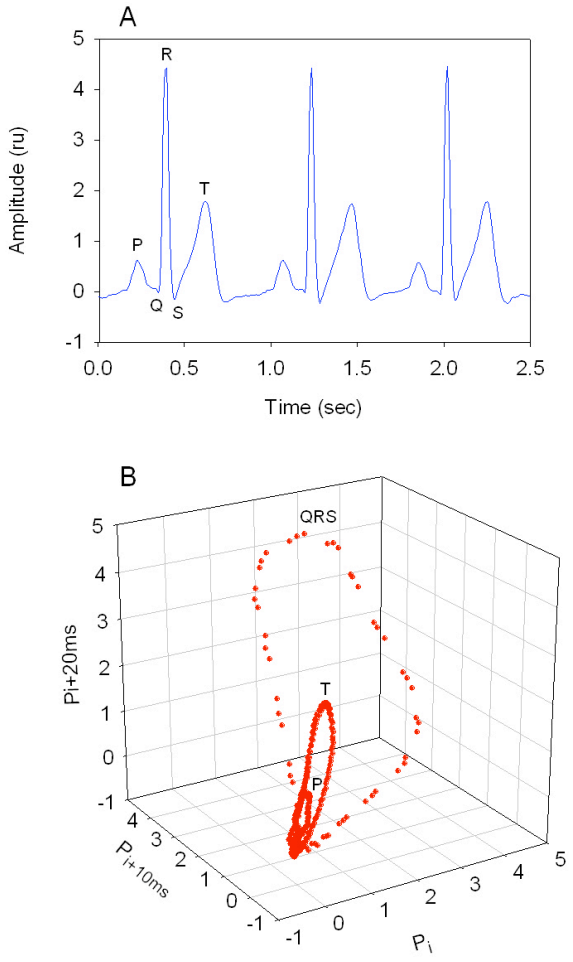

Figure 2.3. (A) Time series of a one-dimensional, lead II electrocardiogram recorded from a normal human volunteer and digitized at a rate of 200 Hz. Displayed are the first three cardiac cycles with characteristic P waves (atrial depolarization), QRS complexes (ventricular depolarization) and T waves (ventricular repolarization). (B) Three-dimensional reconstruction of the ECG signal in phase space by the method of time delays (τ = 10 ms). Each ECG wave (P, QRS, T) forms its own unique loop (three times), returning to isopotential (0,0,0 amplitude units) between waves (T-P interval). Time series data from file ECG (A) with 5 ms per point. Phase-space data from file ECG with DELAY = 2 points (10 ms) or 4 points (20 ms).

higher-dimensional system consisting of multiple coupled variables can be reconstructed from but a single measured variable of that system. That is, the actual dimension of the system (D) is set by a

number of participant variables, but we may only need to measure one of those variables to learn interesting features of the system's underlying dynamics. The reconstruction is performed by defining time-delayed vectors (V_i) of M points (P_i) that are delayed or offset in time (τ). Thus, each point represents a single amplitude (scalar) at a specific instance in time.

$$\text{D-dimensional vector, } V_i = P_i + P_{i+\tau} + P_{i+2\tau} + \ldots + P_{i+(D-1)\tau} \qquad [2.1]$$

Think of what this means graphically for our single-lead ECG signal. If the 1-dimensional data (ECG vector) are plotted against itself twice delayed (τ and 2τ) on a three-axis plot, the signal is promoted into 3-dimensional space as shown in Figure 2.3B. As seen, the morphology of this normal electrocardiogram forms three loops in phase space corresponding to the P, QRS and T waves of the ECG time series. Topologically, these loops are identical to the simultaneous plotting of three orthogonal leads, had they been recorded. That is, the one measured variable (ECG lead II) becomes a surrogate for the two unmeasured variables (ECG leads I & III).

Careful examination of Equation 2.1 explicitly introduces two of the seven recurrence parameters mentioned previously. First we need to know into what dimension the dynamic should be projected, the embedding dimension (M), where M >= D. And second, for M > 1, we need to pick an appropriate delay (τ) between sequential time points in the 1-dimensional signal. It must be appreciated that the selections of embedding dimension and delay are not trivial, but are based on

nonlinear dynamical theory. Moreover, the presence of noise complicates the situation, as will be discussed later.

Embedding dimension (M or EMBED), the first recurrence parameter, can in principle be estimated by the nearest-neighbor methodology of Kennel, Brown, and Abarbanel (1992). Parameter M is increased in integer steps until the recruitment of nearest neighbors of the dynamic under scrutiny becomes unchanging. At this particular value of M, the information of the system has been maximized (and, technically speaking, the attractor has been completely unfolded). Thus, there is no need to explore higher dimensions since no new information would be recruited anyway. This methodology works well on stable and low-noise systems, which are most notably found in mathematical examples such as the Lorenz attractor (Lorenz, 1963). But when it comes to real-world data, noise inflates the dimension (D) (Parker & Chua, 1989), and non-stationarities (transients, drifts) in the system modulate the critical M. Thus, in practice, M > D. Because of these practical limitations, we typically use embedding dimensions of 10 to 20 on biological systems, but no higher. It is a curious fact that when the embedding dimension is set to too high, even random/stochastic systems (which in theory exhibit recurrence only by chance) display strong, yet artifactual, patterns of recurrence.

Delay (τ or DELAY), the second recurrence parameter, should be selected so as to minimize the interaction between points of the measured time series. This, in effect, opens up the attractor (assuming one exists), by presenting its largest profile. An analogy would be the construction of a circle by plotting a sine wave against itself delayed by 90 degrees (whereas delaying by a mere 1 degree would yield a very

thin, slightly bowed line profile). Two common ways of selecting a proper delay include finding the first minimum in either the (linear) autocorrelation function or (nonlinear) mutual information function (Frazer & Swinney, 1986) of the continuous time series. For discontinuous signals (maps as opposed to flows), such as R-R intervals extracted from the continuous ECG signals, the delay is best set to 1 (no points in the time series are skipped). In special cases, parameter τ can also be set to 1 for continuous flows if the goal to is to perform waveform matching (recurrence matching of similar waveforms, point-for-sequential-point). As a corollary to this discussion, Grassberger, Schreiber, and Schaffrath (1991) demonstrated that the delay is a non-critical critical parameter, provided the attractor is sufficiently opened up. When any parameter is non-critical it simply means that the quantitative features of the system are robust and stable against changes in the named parameter. This comes as good news for physiological systems in which we need not over concern ourselves with finding the optimal delay (which anyway is non-existent for transient states), since many delays will suffice for the same system.

The third recurrence parameter is the *range*, defined by the selected starting point (P_{start}) and ending point (P_{end}) in the time series to be analyzed. For an embedded time series ($M > 1$) of N points, it becomes obvious that $M - 1$ embedded points must extend beyond P_{end}. Thus P_{end} can extend no further than $N - M + 1$ points into the available data. In effect, the range defines a window ($W = P_{end} - P_{start} + 1$) on the dynamic under investigation. As will be stressed, short windows focus on small-scale recurrences, whereas long windows focus on large-scale recurrences (see Figure 2.8).

The fourth recurrence parameter is the *norm*, of which there are three selections possible: Minimum norm, maximum norm, and Euclidean norm. As implied by its name, the norm function geometrically defines the size (and shape) of the neighborhood surrounding each reference point. The recurrence area is largest for the max norm, smallest for the min norm, and intermediate for the Euclidean norm (see Marwan, 2003a). (Since a vector must have at least two points, each norm is unique if and only if $M > 1$, else all norms are exactly equivalent for $M = 1$.) But before we can get explicit about norms, it is necessary to be absolutely clear as to how vectors are defined from the 1-dimensional time series. Think of it this way. Take a vector time series (T) of N scalar points (P) and double label the time series as follows:

$$T_i = T_j = P_1, P_2, P_3, P_4, \ldots, P_N. \qquad [2.2]$$

The dual subscripts ($i \neq j$) refer to different points (P_i and P_j) in T_i and T_j when $M = 1$, but to different vectors (V_i and V_j) in T_i and T_j when $M > 1$. Each vector is constructed by starting with an initial point and taking $M - 1$ subsequent points offset by τ (see Equations 2.3 and 2.4 and compare with Equation 2.1). The distances between all possible combinations of i-vectors (V_i) and j-vectors (V_j) are computed according to the norming function selected. The minimum or maximum norm at point P_i,P_j is defined, respectively, by the smallest or largest difference between paired points in vector-i and vector-j ($V_i - V_j$). The Euclidean norm is defined by the Euclidean distance between paired vectors (Equation 2.5).

$$V_i = P_i + P_{i+\tau} + P_{i+2\tau} + \ldots + P_{i+(M-1)\,\tau} \quad [2.3]$$

$$V_j = P_j + P_{j+\tau} + P_{j+2\tau} + \ldots + P_{j+(M-1)\,\tau} \quad [2.4]$$

$$\text{Euclidean distance} = \sqrt{(\Sigma(V_i - V_j)^2)} \quad [2.5]$$

Computed distance values are distributed within a distance matrix DM[j, i] which aligns vertically with T_j and horizontally with T_i (i = 1 to W; j = 1 to W; where maximum W = N – M + 1). The distance matrix has W^2 elements with a long central diagonal of W distances all equal to 0.0. This ubiquitous diagonal feature arises because individual vectors are always identical matches with themselves ($V_i = V_j$ whenever i = j). The matrix is also symmetrical across the diagonal (if vector V_i is close to vector V_j then by necessity vector V_j is close to vector V_i).

The fifth recurrence parameter is the *rescaling* option. The distance matrix can be rescaled by dividing down each element in the distance matrix (DM) by either the mean distance or maximum distance of the entire matrix. In general, DM rescaling allows systems operating on different scales to be statistically compared. Mean distance rescaling is useful in smoothing out any matrix possessing an outlier maximum distance. But maximum distance rescaling is the most commonly used (and recommended) rescaling option, which redefines the DM over the unit interval (0.0 to 1.0 or 0.0% to 100.0%). It is also possible to leave the DM unaltered by not rescaling. In such special cases, DM distances are expressed in absolute units identical to the amplitude units of the input time series (volts, mm Hg, angstroms, seconds, etc.).

The sixth recurrence parameter is the *radius* (RADIUS), which is always expressed in units relative to the elements in the distance matrix, whether or not those elements have been rescaled. In the sea wave example, the radius was actually set to three different values: RADIUS = 0.0, 0.2, and 0.9 ft (Figures 2.2A, B, and C, respectively). In that case we can speak in absolute distances because the distance matrix was never rescaled. In effect, the radius parameter implements a cut-off limit (Heavyside function) that transforms the distance matrix (DM) into the recurrence matrix (RM). That is, all (i, j) elements in DM with distances at or below the RADIUS cutoff are included in the recurrence matrix (element value = 1), but all other elements are excluded from RM (element value = 0). Note carefully that the RM derives from the DM, but the two matrices are not identical. As seen for the wave data (Figure 2.2), as the radius increases, the number of recurrent points increases. Only when RADIUS equals or exceeds the maximum distance is each cell of the matrix filled with values of 1 (the recurrence matrix is saturated). The "shotgun plot" of Figure 2.4 provides a conceptual framework for understanding why an increasing RADIUS captures more and more recurrent points in phase space. Thus, if one becomes too liberal with RADIUS, points (M = 1) or vectors (M > 1) that are actually quite distant from one another will nonetheless be counted as recurrent (the recurrence matrix is too inclusive). Proper procedures for selecting the optimal RADIUS parameter will be described below.

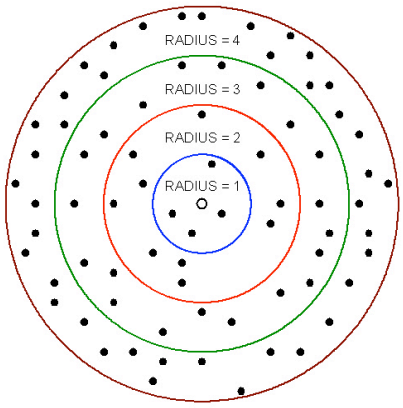

Figure 2.4. Representation of a hypothetical system in higher-dimensional phase space with a splay of points (closed dots) surrounding a single reference point (open dot). The points falling within the smallest circle (RADIUS = 1 distance units) are the nearest neighbors of the reference point. That is, those points are recurrent with the reference point. The second concentric circle (RADIUS = 2 distance units) includes a few more neighbors, increasing the number of recurrences from 4 to 14. Increasing the radius further (RADIUS = 3 or 4 distance units) becomes too inclusive, capturing an additional 20 or 60 distant points as nearest neighbors when, in fact, they are not.

The seventh and last parameter is termed the *line* parameter (LINE). This parameter is important when extracting quantitative features from recurrence plots (see next section), but exerts no effect on the recurrence matrix itself. If the length of a recurrence feature is shorter than the line parameter, that feature is rejected during the quantitative analyses. Typically, the line parameter is set equal to 2 because it takes a minimum of two points to define any line. But it is possible to increase the line parameter (in integer steps) and thereby implement a quantitative filter function on feature extractions, but this is not necessarily recommended.

RECURRENCE QUANTIFICATION

Simply put, recurrence plots, especially colored versions expressing recurrence distances as contour maps, are beautiful to look at (e.g., Figure 2.2C). With little debate, global recurrence plots of time series and signals extant in nature captivate one's attention. Admittedly, such curious and intriguing graphical displays tend more to evoke artistic than scientific appreciation, and rightfully so. Recalling the brief history of recurrence analysis, recurrence plots were originally posited as qualitative tools to detect hidden rhythms graphically (Eckmann et al., 1987). From the outset, color was not the key; rather the specific patterns of multi-dimensional recurrences gave hints regarding the underlying dynamic. Early on it was understood how important it was to hold the radius parameter to small values so as to keep the recurrence matrix sparse. In so doing, emphasis was placed on local recurrences that formed delicate, lacy patterns. All of this is well and good, but the next logical step was to promote recurrence analysis to quantitative status (Zbilut & Webber, 1992; Webber and Zbilut, 1994). Instead of trusting one's eye to "see" recurrence patterns, specific rules had to be devised whereby certain recurrence features could be automatically extracted from recurrence plots. In so doing, problems relating to individual biases of multiple observers and subjective interpretations of recurrence plots were categorically precluded.

We will highlight the fundamental rules of recurrence quantification analysis (RQA) by employing the classic strange attractor of Hénon (1976). This chaotic attractor is a geometrical structure (system) that derives its form (dynamic) from the nonlinear coupling of

two variables. Note in Equation 2.6 that the next data point, X_{i+1}, is a nonlinear function of the previous X_i and Y_i terms (the X_i^2 term provides the nonlinear interaction), whereas in Equation 2.7 the next Y_{i+1} is a linear function of the previous X_i term.

$$X_{i+1} = Y_i + 1.0 - (1.4X_i^2) \quad [2.6]$$

$$Y_{i+1} = 0.3X_i \quad [2.7]$$

We seeded the coupled Hénon variables with initial zero values (e.g., $X_0 = Y_0 = 0.0$) and iterated the system 2000 times to create a sample time series. To make sure the dynamic settled down on its attractor, the first 1000 iterations were rejected as transients. The next 200 iterations of the system are plotted in Figure 2.5 (cycles 1001 through 1200), which shows the complex dynamics of the coupled variables. Plotting Y_i as a function of X_i generates the Hénon strange attractor (Figure 2.6A). It is called an attractor because dynamical points are "attracted" to certain positions on the map and "repelled" from other positions (the white space). Note that the points remain confined within tight limits (± 1.3 for X and ± 0.4 for Y) without flying off to infinity. The dimension of the Hénon attractor is estimated to be around 1.26 (Girault, 1991), which is a fractal or non-integer dimension. Fractal dimensions relate more to the mathematical concept of scaling than real-world dimensions, which must be integers (see Liebovitch & Shehadeh, Chapter 5). Recalling the method of time delays as discussed for the ECG example (Figure 2.3), plotting X_i (current value) as a function of X_{i+1} (next value) topologically reproduces the Hénon

attractor (Figure 2.6B). So does plotting Y_i as a function of Y_{i+1} (Figure 2.6C). These relationships underscore the remarkable power of surrogate variables to adequately substitute for unmeasured variables by using the method of time delays (Takens, 1981).

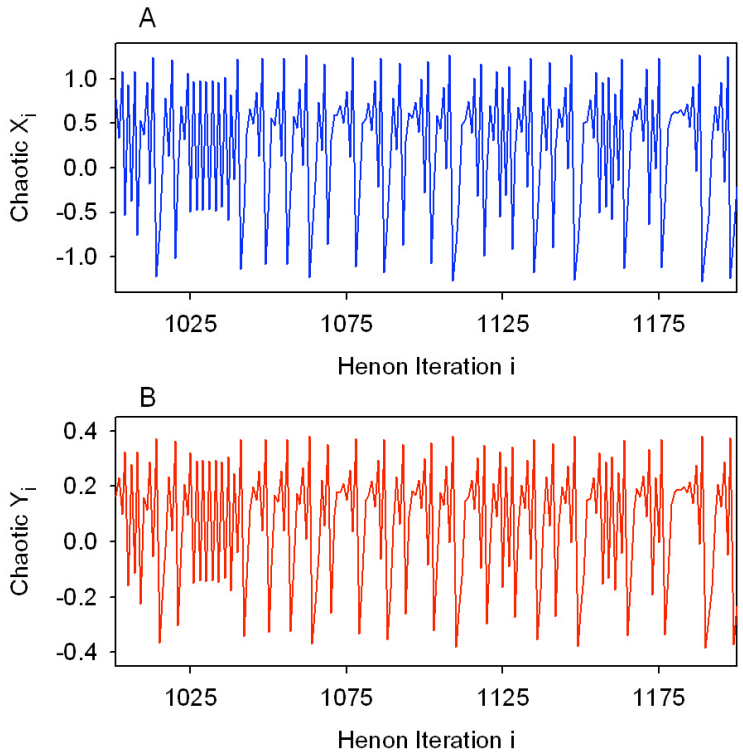

Figure 2.5. Fluctuations of the X_i and Y_i variables comprising the Hénon system in its chaotic mode (Equations 2.6 and 2.7). The first 1000 iterations are rejected before plotting the next 200 iterations (cycles 1001-1200). The dynamic behaviors of both variables are complex, but bounded to the Hénon attractor (see Figure 2.6). The dynamics are also fully deterministic, yet noisy, depending upon the round-off routines implemented by the digital computer that generated the data. Iterated data from files *HENCX* and *HENCY*.

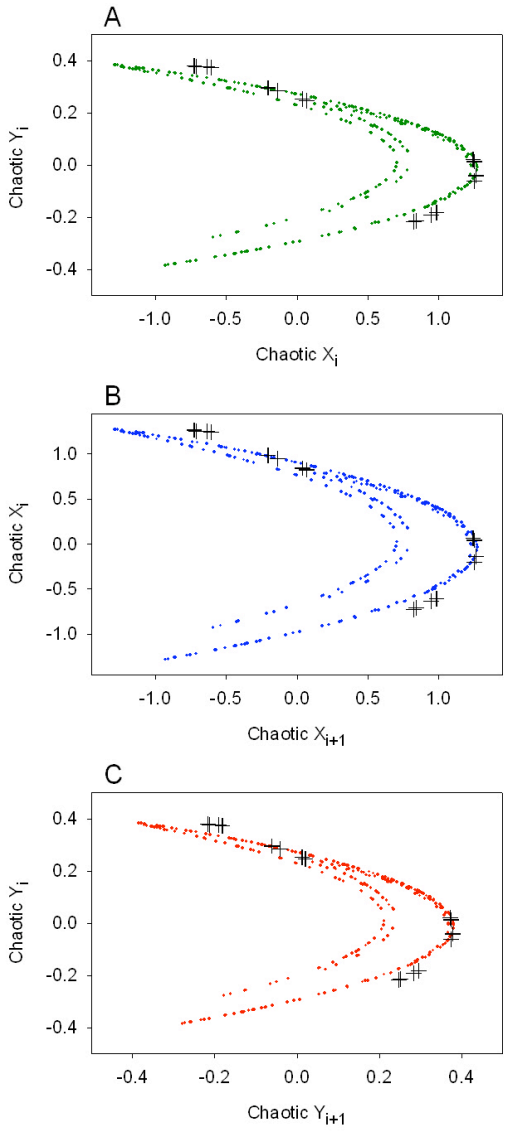

Figure 2.6. Reconstruction of the Hénon strange attractor in phase space by three separate methods. (A) Plotting Y_i versus X_i generates the familiar Hénon strange attractor (dots; Equations 2.6 and 2.7) or 16-point Hénon periodic attractor (crosshairs; Equations 2.18 and 2.19). (B) Plotting X_i versus X_{i+1} reconstructs the topological features of the original Hénon strange attractor by the method of time delays. (C) Plotting Y_i versus Y_{i+1} also reconstructs the attractor. Plots generated from data files *HENCX*, *HENCY*, *HENPX*, *HENPY* (with DELAY = 1 for B and C).

Let us select the Hénon X variable (Figure 2.5A) and generate a recurrence plot of this single variable, as shown in Figure 2.7. The window size (W) is 200 points (e.g., cycles 1001-1200). This is an auto-recurrence plot since the Hénon X variable is being compared with itself (points X_i = points X_j, 3 points at a time since M = 3). Qualitative examination of the symmetrical recurrence plot reveals short line segments parallel to the central diagonal, a cluster of points correspondent to a brief period-2 structure in the dynamic (cycles 1025-1036), and a few isolated points representing chance recurrences. We will focus on the diagonal and vertical structures since from those stem the seven recurrence (dependent) variables or quantifications. Because the recurrence plot is symmetrical across the central diagonal, all quantitative feature extractions take place within the upper triangle, excluding the long diagonal (which provides no unique information) and lower triangle (which provides only redundant information).

The first recurrence variable is *%recurrence* (%REC). %REC quantifies the percentage of recurrent points falling within the specified radius. This variable can range from 0% (no recurrent points) to 100% (all points recurrent). For a given window size W, Equation 2.8 holds true. For the Hénon attractor (Figure 2.7), %REC = 1.201% confirming that the recurrence matrix is sparse (as is desired).

$$\%REC = 100 (\#\text{recurrent points in triangle}) / (W(W - 1) / 2) \quad [2.8]$$

The second recurrence variable is *%determinism* (%DET). %DET measures the proportion of recurrent points forming diagonal line structures. Diagonal line segments must have a minimum length

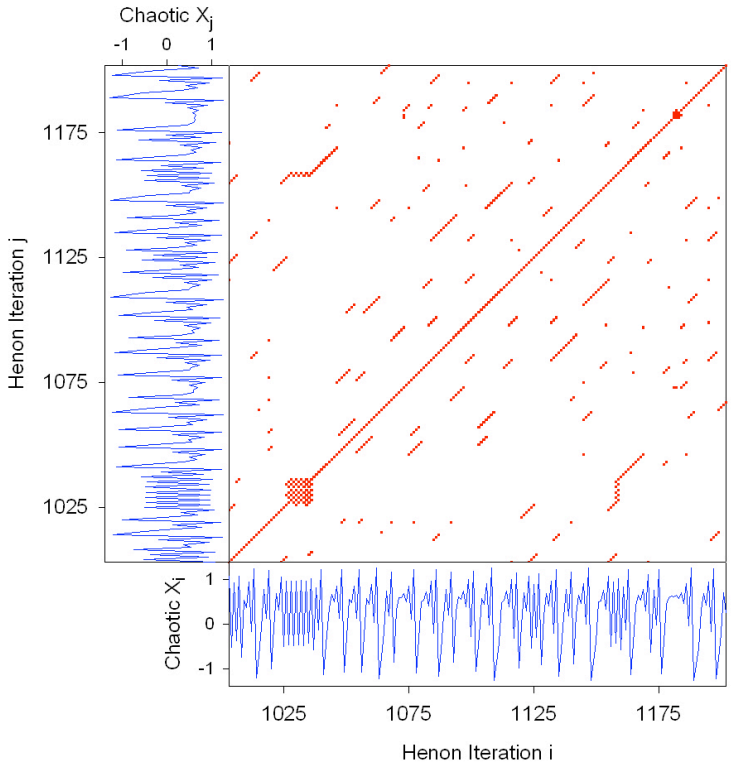

Figure 2.7. Recurrence plot of the Hénon chaotic X variable. The same variable is plotted on the horizontal (chaotic X_i) and vertical axes (chaotic X_j) from iterations of coupled Equations 2.6 and 2.7. When vectors of 3 points (e.g., M = 3) match, recurrent points are plotted at the corresponding (i, j) intersections. The most striking feature of this plot is the short diagonal line structures parallel to the main diagonal. Recurrence data computed from file *HENCX* using program *RQD.EXE*. RQA parameters: P_1-P_{last} = 1001-1200; RANDSEQ = n; NORM = Euclid; DELAY = 1; EMBED = 3; RESCALE = max dist; RADUS = 3; COLORBND = 1; LINE = 2. RQA variables: %REC = 1.201; %DET = 88.703; LMAX = 12; ENT = 2.557; TND = –4.505; %LAM = 2.510; TT = 2.000.

defined by the line parameter, lest they be excluded. The name determinism comes from repeating or deterministic patterns in the dynamic. Periodic signals (e.g. sine waves) will give very long diagonal lines, chaotic signals (e.g. Hénon attractor) will give very short diagonal lines, and stochastic signals (e.g. random numbers) will

give no diagonal lines at all (unless parameter RADIUS is set too high). For the Hénon attractor (Figure 2.7), %DET = 88.703% showing that most of the recurrent points present are found in deterministic structures.

%DET = 100 (#points in diagonal lines)/(#recurrent points) [2.9]

The third recurrence variable is *linemax* (LMAX), which is simply the length of the longest diagonal line segment in the plot, excluding the main diagonal line of identity (i = j). This is a very important recurrence variable because it inversely scales with the most positive Lyapunov exponent (Eckmann et al., 1987; Trulla et al., 1996). Positive Lyapunov exponents gauge the rate at which trajectories diverge, and are the hallmark for dynamic chaos. Thus, the shorter the linemax, the more chaotic (less stable) the signal. For the Hénon attractor (Figure 2.7), LMAX = 12 points.

LMAX = length of longest diagonal line in recurrence plot [2.10]

The fourth recurrence variable is *entropy* (ENT), which is the Shannon information entropy (Shannon, 1948) of all diagonal line lengths distributed over integer bins in a histogram. ENT is a measure of signal complexity and is calibrated in units of bits/bin. Individual histogram bin probabilities (P_{bin}) are computed for each non-zero bin and then summed according to Shannon's equation. For the Hénon attractor (Figure 2.7), ENT = 2.557 bits/bin due to a wide distribution of diagonal line lengths. For simple periodic systems in which all diagonal lines are of equal length, the entropy would be expected to be

0.0 bins/bin (but see Figure 2.12). The units of bits per bin come from taking the base-2 logarithm. For further discussion of ENT see Pellechia and Shockley (Chapter 3).

$$ENT = -\sum(P_{bin})\log_2(P_{bin}) \quad [2.11]$$

The fifth recurrence variable is *trend* (TND), which quantifies the degree of system stationarity. If recurrent points are homogeneously distributed across the recurrence plot, TND values will hover near zero units. If recurrent points are heterogeneously distributed across the recurrence plot, TND values will deviate from zero units. TND is computed as the slope of the least squares regression of %local recurrence as a function of the orthogonal displacement from the central diagonal. Multiplying by 1000 increases the gain of the TND variable. For the Hénon attractor (Figure 2.7), TND = –4.505 units, which is within the ± 5 units, confirming system stationarity (Webber et al., 1995) as achieved by rejecting the first 1000 points.

TND = 1000(slope of %local recurrence vs. displacement) [2.12]

The sixth and seventh recurrence variables, *%laminarity* (%LAM) and *trapping time* (TT), were introduced by Marwan, Wessel, Meyerfeldt, Schirdewan, and Kurths (2002). %LAM is analogous to %DET except that it measures the percentage of recurrent points comprising vertical line structures rather than diagonal line structures. The line parameter still governs the minimum length of vertical lines to be included. TT, on the other hand, is simply the average length of

vertical line structures. For the Hénon attractor (Figure 2.7), %LAM = 2.510% and TT = 2.000, showing that vertical line structures are not common for this system.

%LAM = 100(#points in vertical lines)/(#recurrent points) [2.13]

TT = average length of vertical lines ≥ parameter line [2.14]

Recurrence plots and recurrence quantifications are strongly dependent on the sequential organization of the time series or data string. By contrast, standard statistical measures such as mean and standard deviation are sequence independent. Random shuffling of the original sequence destroys the small-scale structuring of line segments (diagonal as well as vertical) and alters the computed recurrence variables, but does not change the mean and standard deviation. A good analogy would be that of Morse code. Random shuffling of the dots and dashes would not change the percentage of dots and dashes in the code, but it would certainly alter/destroy the encoded message! This important idea will be expanded upon when we discuss linguistic texts and protein codes.

RECURRENCE EPOCHS

So far we have demonstrated that time series data (linear vectors of sequential scalar measurements of length N) can be embedded into higher dimensional space by the method of time delays (Takens, 1981). Distances between all possible vectors are computed and registered in a distance matrix, specific distance values being based on the selected

norm parameter. A recurrence matrix (RM) is derived from the distance matrix (DM) by selecting an inclusive radius parameter such that only a small percentage of points with small distances are counted as recurrent (yielding a sparse RM). The recurrence plot (RP), of course, is just the graphical representations of RM elements at or below the radius threshold. Seven features (recurrence variables) are extracted from the recurrence plot within each window (W) of observation on the time series. The question before us now is how can these recurrence variables be useful in the diagnosis of dynamical systems?

Whenever any dynamic is sampled, we are taking a "slice of life," as it were. The dynamic was "alive" before we sampled it, and probably remained "alive" after our sampling. Consider, for example, the EMG signal recorded from the biceps muscle of a normal human volunteer and its attendant recurrence plot in Figure 2.8 (Webber, Schmidt, & Walsh, 1995). The focus is on the first 1972 points of the time series digitized at 1000 Hz (displayed from 37 ms to 1828 ms). But how might these digitized data be processed in terms of recurrence analysis? It would certainly be feasible to perform recurrence quantifications within the entire window (W_{large} = 1972 points) as represented by the single, large, outer RM square. On the other hand, the data can be windowed into four smaller segments (W_{small} = 1024 points) as represented by the four smaller and overlapping RM squares. In the latter case the window offset of 256 points means the sliding window jogs over 256 points (256 ms) between windows. Two effects are at play here. First, larger windows focus on global dynamics (longer time frame) whereas smaller windows focus on local dynamics

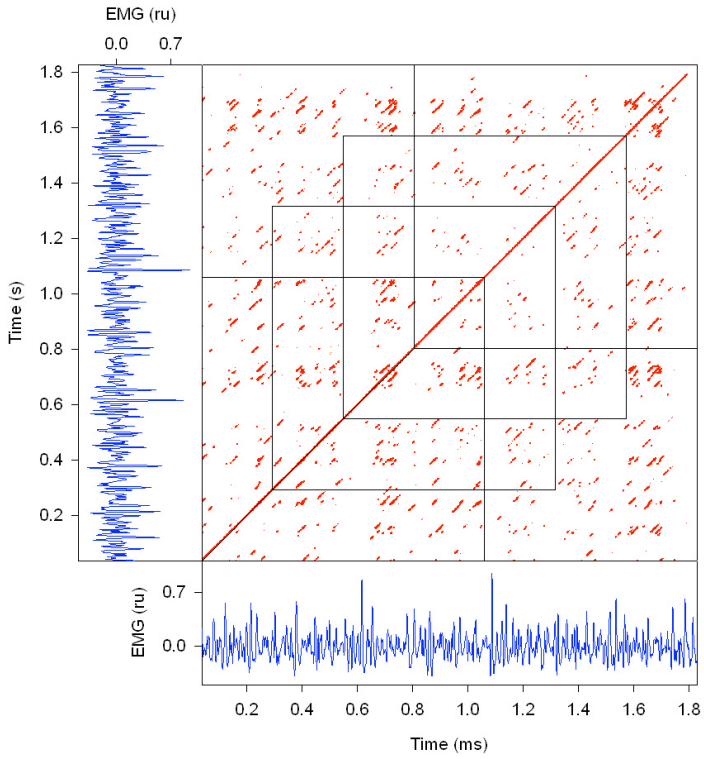

Figure 2.8. Windowed recurrence analysis of resting biceps brachii EMG signal. The large outer square displays the large scale recurrence plot (W = 1792 = N points). The four small inner squares (epochs) block off the small scale recurrence plots (W = 1024 < N) with an offset of 256 points between windows. Recurrence data computed from file *EMG* using program *RQD.EXE*. RQA parameters: P_1-P_{last} = 1-1972 (for large square) or 1-1024, 257-1280, 513-1536, 769-1792 (for small squares); RANDSEQ = n; NORM = Euclid; DELAY = 4; EMBED = 10; RESCALE = max dist; RADUS = 15; COLORBND = 1; LINE = 2. RQA variables (for large square): %REC = 0.335; %DET = 60.905; LMAX = 118; ENT = 1.711; TND = –0.129; %LAM = 55.660; TT = 2.501. RQA variables (for small squares, respectively): %REC = 0.471, 0.407, 0.331, 0.311; %DET = 68.560, 65.603, 66.474, 68.140; LMAX = 118, 118, 118, 59; ENT = 1.753, 1.778, 1.751, 1.572; TND = –0.488, –0.663, –0.644, –0.464; %LAM = 59.635, 54.435, 45.759, 44.506; TT = 2.454, 2.500, 2.396, 2.425.

(shorter time frame). Second, larger window offsets yield lower time-resolution RQA variables, whereas smaller window offsets yield higher time-resolution variables. Remember, seven RQA variables are computed (extracted) from each RM (or RP). By implementing a sliding window design, each of those variables is computed multiple times,

creating seven new derivative dynamical systems expressed in terms of %REC, %DET, LMAX, ENT, TND, %LAM, and TT. Alignment of those variables (outputs) with the original time series (input) (adjusting for the embedding dimension, M) might reveal details not obvious in the 1-dimensional input data.

Here are the important details of this the muscle fatigue experiment performed by Webber et al. (1995) which illustrate these fundamental rules of sliding windows (termed *epochs*). While seated comfortably, normal human volunteers were instrumented for the recording of surface EMG signals from the biceps brachii as shown in Figure 2.9A. Subjects were asked to hold their forearm parallel to the floor and their elbow at 90°. A 1.4 kg weight was placed in the open palm and a control EMG recording was digitized at 1000 Hz. After 60 seconds of recording, the weight load was increased to 5.1 kg, which led to total muscle fatigue in 1 to 6 minutes (or 2.8 minutes for the example subject in Figure 2.9), depending upon the biceps muscle mass of the subject. The experiment was designed to compare the performance of nonlinear RQA and linear spectral analysis on identical EMG signals. Might the two techniques have differential sensitivities?

The recorded time series (N = 227,957 points) was partitioned in shorter windows (W = 1024) or epochs, each 1.024 seconds long. Adjacent windows were offset by 256 points (75% overlap), fixing the time resolution to 256 ms. Spectral features and recurrence quantifications were then computed for each of the 887 sliding windows. As shown in Figure 2.9B and 2.9C, respectively, the spectral center frequency (F_C) and recurrence %DET were stable during the 60 second, low-weight control period. For statistical purposes, 95%

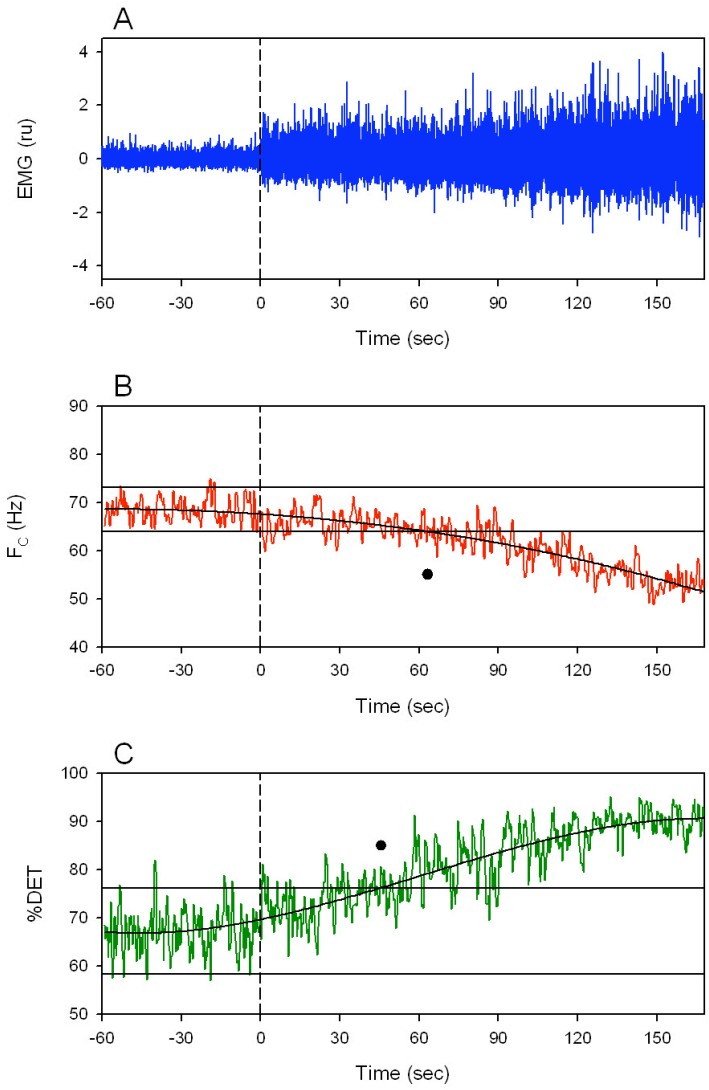

Figure 2.9. Muscle fatigue experiment in a human volunteer, designed to force the system through a series of state changes until task failure occurs. (A) Bipolar surface EMG recording from the biceps brachii muscle during light-weight loading (1.4 kg) before time zero, and heavy-weight loading (5.1 kg) starting at time zero. After 60 sec of control (steady-state dynamics), the subject was forced onto a trajectory (transient dynamic) ending in task failure over the next 167 sec. (B) Spectral center frequency (F_C) remains constant during the light-weight loading, but slowly decreases during the heavy-weight loading. The first spectral detection of fatigue occurs at 63.3 sec when the 3rd degree polynomial breaks out of the control 95% confidence limits (dot). (C) Recurrence variable %DET also remains constant during the light-weight loading, but increases during the heavy-weight loading. Fatigue is detected by %DET after only 45.6 sec (dot) or 28% sooner than F_C. EMG digitized at a rate of 1000 Hz. Recurrence data computed from data file *EMG* using program *RQE.EXE*. RQA parameters: P_1-P_{last} (first epoch) = 1-1024; SHIFT = 256; #EPOCHS = 887; RANDSEQ = n; NORM = Euclid; DELAY = 4; EMBED = 10; RESCALE = max dist; RADUS = 15; LINE = 2.

confidence limits were drawn for each control trace, and a 3rd degree polynomial was constructed through each data set. Increasing the load, however, perturbed the steady-state dynamics and set the biceps' contractile machinery on a transition trajectory toward muscle fatigue and ultimate task failure. Examination of the output data shows that during the fatiguing process, F_C decreased whereas %DET increased. Both variables can be interpreted as indicators of larger motor unit recruitment and synchronization, but that is not the point being made here. What is significant is the fact that the %DET broke out of its 95% confidence limit before F_C broke out of its 95% confidence limit (e.g. at 45.6 sec versus 63.3 sec after the heavy loading, respectively, or 28% sooner). It can be concluded that whereas both spectral and recurrence strategies are responsive to dynamical changes in physiological systems such as fatiguing muscle, recurrence quantification is substantially more sensitive. In other words, subtle dynamical departures from "steady state" occurring in time series data might be delayed or even missed by spectral tools, but detected sooner and/or more accurately by recurrence tools.

This EMG example illustrates the power of sliding recurrence windows, but we glanced over the determination of the several important recurrence parameters. As mentioned, each window consisted of 1024 points (range). But we also selected the Euclidean norm, maximum distance rescaling, and a line of 2 (all typical choices). But what about the delay, radius, and embedding dimension parameters—how were they selected? First, to estimate an ideal delay time, the control EMG data (58 windows of non-overlapping, adjacent windows, 1.024 sec each) were subjected to autocorrelation analysis.

The average delay, based on the first zero crossing of the autocorrelation function (a zero value indicates no correlation), was found to be 4 digitized points or 4 ms. Second, to estimate the proper radius threshold, the beginning control EMG data (1 window or epoch or 1024 points) were subjected to recurrence scaling analysis. In this case, recurrence variables were recomputed for a family of radius values from 0% to 100% in steps of 1% (of the maximum distance in the distance matrix). Figure 2.10 depicts the results with respect to %REC and %DET. With increasing RADIUS values, %REC increased smoothly to its maximum, following either a sigmoidal curve with linear scaling (Figure 2.10A) or a more linear curve with double logarithmic scaling (Figure 2.10B). On the other hand, %DET exhibited a hitch or shelf with a first local minimum at a radius of 17%. This oddity is due to the faster recruitment of isolated recurrent points than points contributing to diagonal line structures as RADIUS is incremented (Figure 2.10C; see Equation 2.9).

There are three guidelines for selecting the proper radius (in order of preference): (1) RADIUS must fall with the linear scaling region of the double logarithmic plot; (2) %REC must be kept low (e.g., 0.1 to 2.0%); and (3) RADIUS may or may not coincide with the first minimum hitch in %DET. Weighing all three factors together, a radius of 15% was selected for the example EMG data (vertical dashed lines in Figure 2.10), which fits all three criteria. Because there are mathematical scaling rules linking log(%REC) with log(RADIUS), as will be discussed below, the first guideline for RADIUS selection is preferred. In contrast, since there are no known rules describing the hitch region in %DET, this latter method must be applied with caution—user beware.

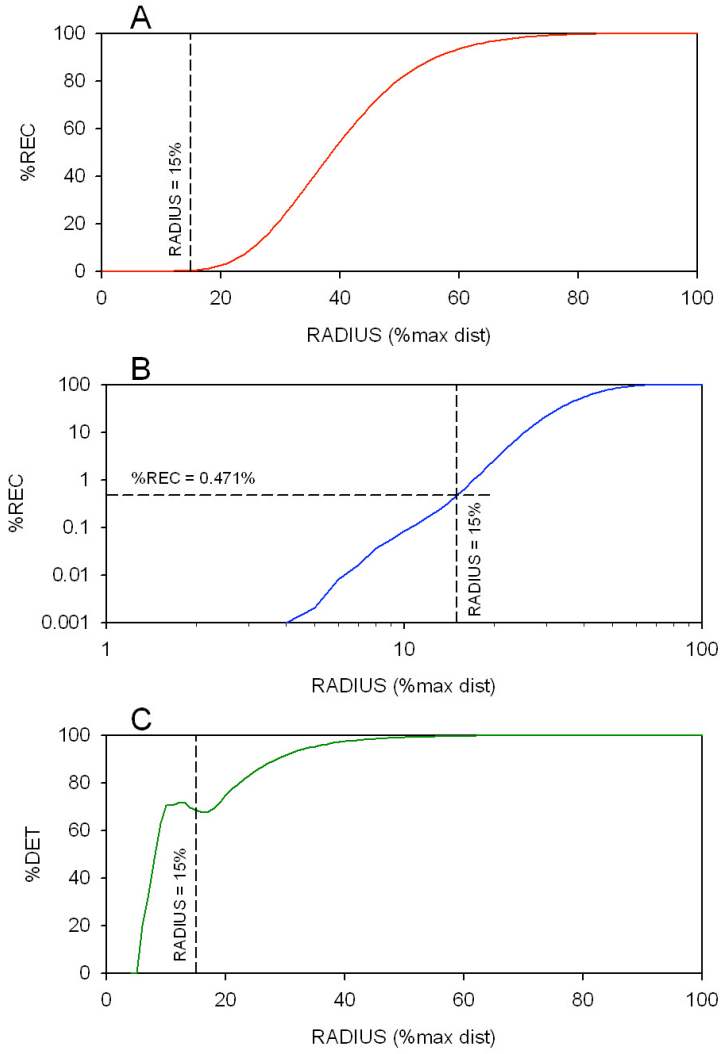

Figure 2.10. Methods for selecting the proper radius parameter for recurrence analysis of the control EMG recording. (A) With step increases in RADIUS, the density of recurrence points (%REC) increases along a sigmoid curve (M = 10). (B) Double-logarithmic plot of %REC as a function of RADIUS defines a linear scaling region from RADIUS = 8% to 15%. RADIUS is selected at 15% where %REC is 0.471% (sparse recurrence matrix). (C) Linear plot of %DET as a function of RADIUS showing a short plateau and small trough near RADIUS = 15% which may or may not be coincidental. Recurrence data computed from file *EMG* using program *RQS.EXE*. RQA parameters: P_1-P_{last} = 1-1024; RANDSEQ = n; NORM = Euclid; DATA MIN = DATA MAX = 4; EMBED MIN = EMBED MAX = 10; RESCALE = max dist; RADUS MIN = 0; RADIUS MAX = 100; RADIUS STEP = 1; LINE = 2.

The third parameter requiring explanation is the embedding dimension. Why did we set M = 10? The mathematics underlying the distance matrix are equivalent to the correlation integral implemented by Grassberger and Procaccia (1983) for dimensional analysis of dynamical systems. Theoretically, the Grassberger-Procaccia dimension (GPD) is a measure of the number of independent variables participating in the system at any given instant. Thus, GPD is another measure of complexity, since the greater the number of participant variables, the more complex the system. Practically, the G-P dimension can be estimated by observing how the number of recurrences (#REC) scales with increases in absolute radius (R), as shown by Equation 2.15. The exponential form of this equation is easily converted to its linear form by taking the logarithm of both sides, yielding Equation 2.16. Then, substitution into this equation of %recurrence (%REC) for #REC and relative radius (RADIUS) for absolute radius (R), respectively, gives Equation 2.17.

$$\#REC = R^{GPD} \qquad [2.15]$$

$$\log(\#REC) = \log(R)GPD \qquad [2.16]$$

$$\log(\%REC) = \log(RADIUS)GPD \qquad [2.17]$$

The G-P Dimension is easily computed by taking the ratio (or slope) of $\Delta\log(\%REC)$ to $\Delta\log(RADIUS)$ over a linear scaling region, as discussed by Mayer-Kress and Holzfuss (1987). Such a double-logarithmic plot is illustrated in Figure 2.11A for embedding

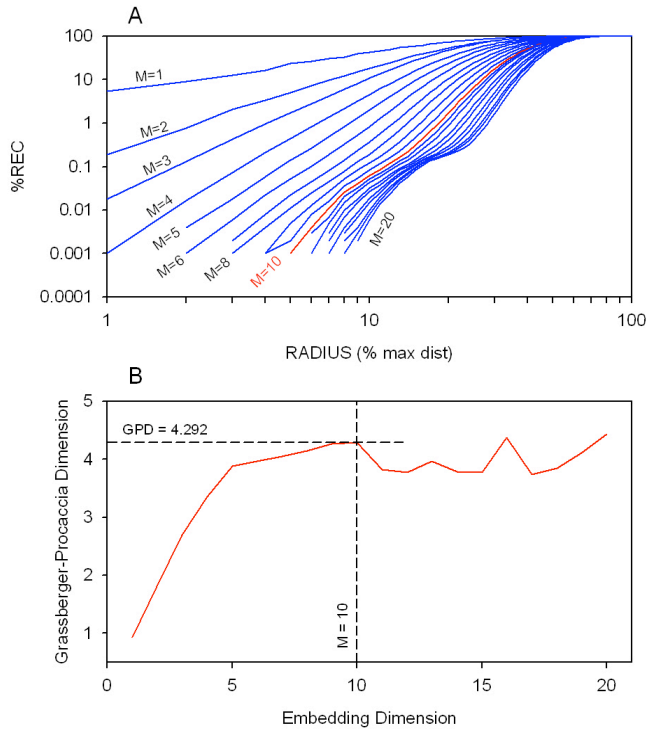

Figure 2.11. Relationship between log(%REC) and log(RADIUS) over a range of embedding dimensions (M = 1 to 20) for the control EMG recording. (A) Each curve in the family of curves has a linear scaling region that is used to estimate the Grassberger-Procaccia dimension (GPD) when the slope becomes unchanging with increases in M. The dashed line refers to the same line plotted in Figure 2.10B at M = 10. (B) GPD plotted as a function of embedding dimension saturates at GPD = 4.292 when M = 10, the proper embedding for this dynamic. Recurrence data computed from file *EMG* using program *RQS.EXE*. RQA parameters: P_1-P_{last} = 1-1024; RANDSEQ = n; NORM = Euclid; DATA MIN = DATA MAX = 4; EMBED MIN = 1; EMBED MAX = 20; RESCALE = max dist; RADUS MIN = 0; RADIUS MAX = 100; RADIUS STEP = 1; LINE = 2.

dimensions ranging from 1 to 20. As shown in Figure 2.11B, as the embedding dimension (M) increases, the slope increases to a "plateau" of GPD = 4.292 (a fractal dimension) starting at M = 10. Further embeddings do not result in any further increases in GPD. This is the reason why we selected M = 10. As is most often the case for real data, it should be recognized that M > GPD. The reason for this is that noise artificially inflates the dimension. Parka and Chua (1989) stated

that for noisy systems, the embedding dimension maximizes at M = 2 × GPD + 1. An M of 10 for our EMG signal is very close to this theoretical limit (M = 2 × 4.292 + 1 = 9.6). There are numerous practical problems associated with the estimation of M, including non-stationary dynamics, high-dimensional attractors, and the presence of noise. For example, inspection of the log-log plots (Figure 2.11B) shows a worsening "double hump" of unknown origin in the curves for M > 10. Therefore, we typically bypass any G-P analysis or nearest-neighbor strategy, and usually set parameter M to 10, but never higher than 20, for real data.

RECURRENCE INTERVALS

Recurrence intervals (or recurrence times) quantify the perioidicities expressed by dynamical systems. By way of one mundane example, it is proper to say that the recurrence interval (or recurrence time) for the earth's sun is 24 hours, day in and day out. But for heuristic purposes, let us revisit the coupled Hénon equations discussed above (Equations 2.6 and 2.7) in which the constant multiplier of the nonlinear term X_i^2 is changed from 1.4 to 1.054 as follows:

$$X_{i+1} = Y_i + 1.0 - (1.054X_i^2), \qquad [2.18]$$

$$Y_{i+1} = 0.3X_i. \qquad [2.19]$$

Such minor tweaking of the equation converts the Hénon chaotic attractor into the Hénon 16-point periodic attractor in phase space (see 16 crosshairs in Figures 2.6A, B, & C). Expressing this periodic

attractor in recurrence space, however, produces a series of parallel lines spanning from border to border as shown in Figure 2.12. Recurrence interval analysis verifies that the vertical spacing between recurrent points throughout the entire plot (including recurrent points in the upper and lower triangles, as well as the central diagonal) is a perfect 16 points, as expected. Since the border effectively truncates diagonal lines to different lengths, an artifactual ENT > 0.0 bit/bin is observed.

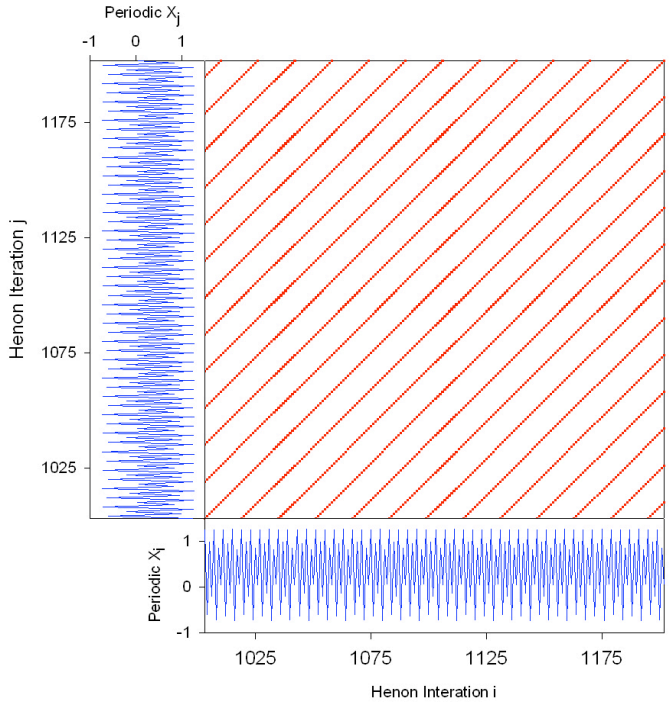

Figure 2.12. Recurrence plot of the 16-point Hénon periodic X variable. The same variable is plotted on the horizontal (periodic X_i) and vertical axes (periodic X_j) from iterations of coupled Equations 2.18 and 2.19. When vectors of 3 points (e.g. M = 3) match, recurrent points are plotted at the corresponding (i,j) intersections. The most striking feature of this plot is the long diagonal line structures parallel to the main diagonal and offset by exactly 16 points. Recurrence data computed from file *HENPX* using program *RQD.EXE*. RQA parameters: P_1-P_{last} = 1001-1200; RANDSEQ = n; NORM = Euclid; DELAY = 1; EMBED = 3; RESCALE = max dist; RADUS = 0.5; COLORBND = 1; LINE = 2. RQA variables: %REC = 5.789; %DET = 100.000; LMAX = 184; ENT = 3.585 (line truncation effect); TND = 12.449; %LAM = 0.000; TT = undefined.

Moving from theoretical mathematics to practical physiology, it is important to demonstrate the power and utility of recurrence interval analysis on revealing subtle features in human ectroencephalographic (EEG) signals. To illustrate this, EEG data from a normal quiescent subject were obtained from a local clinical electrophysiology laboratory. The subject was instrumented with 21 active unipolar electrodes referenced to the nose according to the standard 10-20 EEG recording system (electrodes spaced at intervals 10%-20% of head circumference) (Misulis & Head, 2003). The signals were digitized at 500 Hz and bandpass filtered (0.15 Hz - 70.0 Hz). However, instead of selecting just one of the active electrode sites for analysis, Euclidean distances (ED) were computed for each instance in time (every 2 ms) across all 21 electrodes (E_n) according to Equation 2.20. In effect, an [N,21] matrix of 21 parallel vectors was collapsed into a single [N] vector time series with N points.

$$ED_i = \sqrt{(E_{1i}^2 + E_{2i}^2 + E_{3i}^2 + \ldots + E_{20i}^2 + E_{21i}^2)} \qquad [2.20]$$

Recurrence analysis was conducted on 2000 points (4.0 s) of the composite EEG signal (Euclidean vector), which is plotted horizontally and vertically in Figure 2.13. Because the signal was already projected into higher dimensional space (D=21), it was inappropriate to set the embedding dimension to anything other than one (M = 1). The minimum norm was chosen and the delay parameter was set equal to one ($\tau = 1$), but neither parameter was critical since with an embedding dimension of one, no points were time delayed. The radius was set to 0.2% of the maximum distance rescaling, insuring that %REC < 1%.

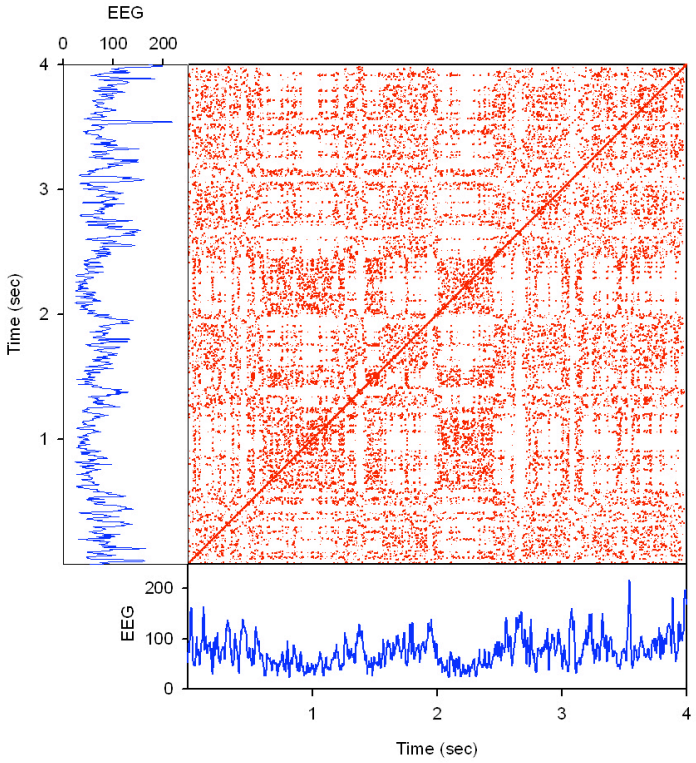

Figure 2.13. Recurrence interval analysis of a normal human electroencephalogram (EEG) digitized at 500 Hz. The time series data are derived from computing the Euclid distances across 21 simultaneously recorded leads of the 10-20 system of electrodes positioned around the skull. Voltages were updated at each instant in time (2 msec) for 40 sec (2000 data points) for recurrence analysis. The recurrence plot has both fine-scale and large-scale features that were captured by measuring the vertical time interval between all recurrent points (see Figure 2.14). Recurrence data computed from file *EEG* using program *RQD.EXE*. RQA parameters: P_1-P_{last} = 1-2000; RANDSEQ = n; NORM = min norm; DELAY = 1; EMBED = 1; RESCALE = max dist; RADIUS = 0.2; COLORBND = 1; LINE = 2. RQA variables: %REC = 0.804; %DET = 7.318; LMAX = 5; ENT = 0.445; TND = –0.102; %LAM = 11.207; TT = 2.087. These EEG data were kindly provided by Lukasz Konopka, Ph.D., Director of Biological Psychiatry, Hines V.A., Hines, IL 60141.

The recurrence plot for this system (Figure 2.13) reveals a much more complex structuring than that observed with the Hénon 16-point periodic system (Figure 2.12). In fact, the seven recurrence variables were quantified for this EEG signal as follows: %REC = 0.804%; %DET = 7.318%; LMAX = 5; ENT = 0.445; TND = –0.102; %LAM = 11.207%; TT

= 2.087. The homogeneous distribution of recurrent points is quantified by the near zero TND value, indicating the stationary state of the EEG signal in this individual. The %DET value indicates that the signal has deterministic features arising from repeated (recurrent) EEG waves at various frequencies. Likewise, the %LAM value reveals significant laminate structuring of recurring dynamical features in the vertical plane (strings of multiple j-points recurring with single i-points). However, it is the vertical spacing between recurrent points (recurrence intervals) that is of interest to us.

Recurrence quantification interval (RQI) analysis was conducted on this example EEG signal using the exact same parameter settings as indicated above. The distribution of recurrence intervals is plotted in a double logarithmic histogram in Figure 2.14. Of the 32,142 intervals counted, 2,075 (6.46%) recurrence intervals are located in the first bin at 2 ms. These points are usually excluded as noise since they come from adjacent points forming vertical line structures (whence see %LAM). Recurrence intervals spanning 4 to 398 ms were distributed rather uniformly, but over the range from 400 through 1,600 msec the recurrence counts scaled with recurrence time. The remainder of intervals from 1,602 to 3,398 ms contained mostly single-digit counts and comprised the noise floor beyond the scaling region. Within the scaling regions, however, slope (S) defines the scaling relationship between the number of intervals (#INT) and interval length (L).

$$\#INT = L^S \qquad [2.21]$$

$$\log(\#INT) = \log(L)S \qquad [2.22]$$

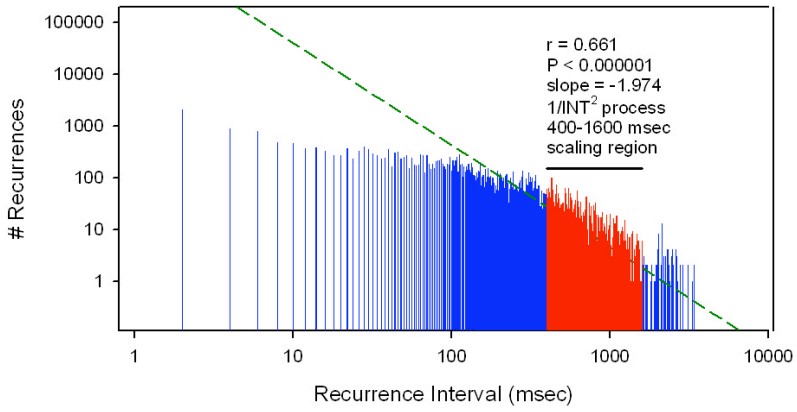

Figure 2.14. Double-logarithmic scaling relation between number of recurrence intervals (tally counts) and duration of recurrence intervals (ms) computed from a normal EEG signal (Figure 2.13). A scaling relation spans the range 400 to 1600 ms and has a significant negative slope ($p < 0.0000001$) of –1.974 (dashed line) indicative of a $1/INT^2$ process. Recurrence data computed from file *EEG* using program *RQI.EXE*. RQA parameters: P_1-P_{last} = 1-2000; RANDSEQ = n; NORM = max norm; DELAY = 1; EMBED = 1; RESCALE = max dist; RADUS = 0.2.

The linear scaling region (Figure 2.14) has a negative slope S = –1.974, which is consistent with a $1/INT^2$ process (where INT is the recurrence interval) and is highly significant ($p < 0.000001$) for the 380 points defining the scaling region. These data indicate that there are scaling rules in place for the lowest EEG frequency (delta < 4 Hz), but not the higher frequencies (beta > 13 Hz; alpha > 8 Hz; theta > 4 Hz) (Misulis & Head, 2003). This type of RQI analysis is analogous to uncovering $1/f$ scaling rules, but in the latter case the lower frequencies (longer intervals) carry most of the power (Bassingthwaighte et al., 1994; see also Aks, Chapter 7, and Liebovitch & Shehadeh, Chapter 5).

Thomasson, Heoppner, Webber, and Zbilut (2001) and Thomasson, Webber, and Zbilut (2002) performed RQI analysis on

human EEG signals and were able to demonstrate different scaling regions for control EEGs versus pre-ictal EEGs. That is, just prior to seizure activity, the scaling relation became more correlated (steeper negative slope), consistent with a self-organizing process leading to synchronized and focal brain activity. These studies provide evidence that subtle recurrence changes in the electrical dynamic may forecast seizure states in the brain.

CROSS RECURRENCE

So far we have been speaking of recurrence quantitative analysis from the single signal perspective. That is, in RQA recurrence patterns are sought within individual signals in the spirit of autocorrelation. However, in the spirit of cross correlation, it is possible to detect recurrence patterns shared by paired signals by cross recurrence analysis (KRQA) (Zbilut, Giuliani, & Webber, 1998a; Marwan et al., 2002; Marwan 2003a; see also Shockley, Chapter 4). The mathematics of cross recurrence, as well as the parameters and variables of cross recurrence, all are the same as explained for auto-recurrence. There are two principle differences, however. First, in KRQA distances are computed between two different signals. It is assumed that the two signals arose from coupled systems, were sampled simultaneously at the same digitization rate (which prohibits the drifting of one signal with respect to the other), and are on the same amplitude scale (which permits low distances between signals to be computed). The last requirement can be achieved by rescaling the input data over the unit interval (minimum:maximum mapped to 0.0:1.0), provided that neither of the paired input data streams possess strong nonstationaity (upward

or downward drifts). Second, in KRQA the shared symmetry between the upper and lower triangles of the auto-recurrence plot is lost. In fact the entire central line of identity vanishes. Because of these expected differences from auto-RQA, quantitative cross-recurrence quantifications must be made across the entire matrix (plot), not just the upper half (upper triangle).

Shockley, Butwill, Zbilut, and Webber (2002) performed a very simple experiment on mechanically coupled oscillators. A tray (which served as a driver), filled with fluids of differing viscosities (oil, syrup, or honey), was set into reciprocal, sine-wave motion by a strong sinusoidal motor. A rotor blade (the follower—what was driven by the driver) was positioned within the viscous fluid and was set into independent motion by a pulley system and falling weight (gravity activated). The position of the tray and rotor were monitored by separate motion-tracking sensors and digitized at 60 Hz. Four experimental runs were performed at each of three viscosities. Transients due to acceleration were rejected and 600 points of steady state data (10 s) were collected for each trial. KRQA was performed using the driver-tray as the i-signal (i-vector, V_i) and the follower-rotor as the j-signal (j-vector, V_j). The cross recurrence plot for one of the trials at a medium coupling viscosity is presented in Figure 2.15 (M = 5; DELAY = 1; RADIUS = 2.0%). The long diagonal, always present for auto-recurrence plots (e.g., Figures 2.2, 2.7, 2.8, 2.12, and 2.13), is noticeably absent. But short diagonals appear in the plot wherever waveform coupling occurs between the driver (independent and constant frequency) and rotor (dependent and variable frequency).

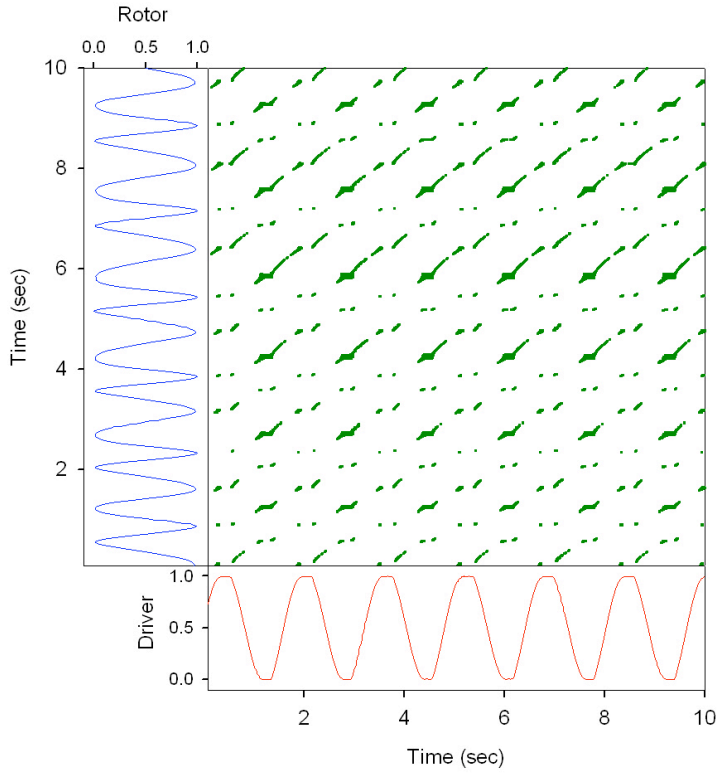

Figure 2.15. Cross recurrence plot of coupled oscillators in a low-viscosity coupling. The positions of the different oscillators are plotted along the horizontal axis (driver oscillator) or vertical axis (rotor oscillator). When vectors of 5 points each match (e.g. M = 5), recurrent points are plotted at the corresponding i,j intersections. The most striking feature of this plot is the unusual distribution of recurrent points reflective of various phasic couplings between the two oscillators. Recurrence data computed from files *DRIVER* and *ROTOR* using program *KRQD.EXE*. RQA parameters: P_1-P_{last} = 1-596; RANDSEQ = n; NORM = Euclid; DELAY = 1; EMBED = 5; RESCALE = max dist; RADUS = 2; COLORBND = 1; LINE = 2. RQA variables: %REC = 1.480; %DET = 94.103; LMAX = 24; ENT = 3.041; TND = –0.813; %LAM = 74.834; TT = 3.300.

Cross recurrence interval analysis (KRQI) on the coupled oscillators results in the frequency spectrum plotted in Figure 2.16. To accomplish this, recurrence intervals were transformed to the frequency domain by taking their reciprocals. For spectral comparison, the Fast Fourier transform (FFT) spectrum is computed on

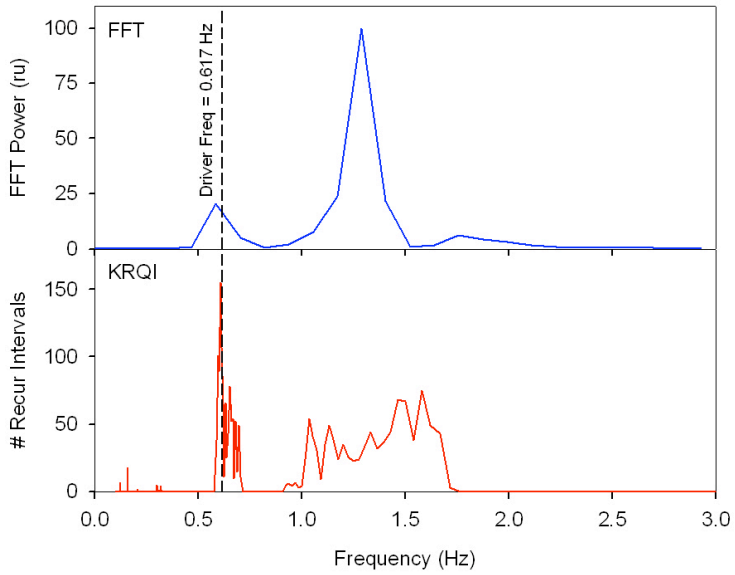

Figure 2.16. Frequency characteristics of the low-viscosity coupled driver-rotor system from linear (FFT) and non-linear (KRQI) perspectives. Spectral analysis (FFT) of the rotor dynamic shows a dominant (uncoupled) frequency faster than the driver frequency at low resolution. Cross recurrence analysis (1/KRQI) reveals similar features but with greater details at high resolution. For example, the high frequency peak is splayed out over a wider frequency band due to subtle nonlinear interactions not detected by FFT. Recurrence data computed from coupled files *DRIVER* and *ROTOR* using program *KRQI.EXE*. RQA parameters: P_1-P_{last} = 1-596; RANDSEQ = n; NORM = Euclid; DELAY = 1; EMBED = 5; RESCALE = max dist; RADUS = 2; LINE = 2.

the rotor data only. The linear FFT spectrum reports two peaks, a low amplitude peak near the driver frequency (dashed line), and a high amplitude peak at a higher frequency (non-harmonic). The nonlinear KRQI spectrum provides much more details on the partially coupled system. More spectral power is found at the higher, uncoupled frequency, but the frequency band is splayed out due to nonlinear interactions between the rotor and driver. At the lower, coupled frequency (dashed line), the KRQI resolution is superior to the FFT resolution. More importantly, subtle changes in relative viscosity from

0.693 to 0.711 units (1.00 units for high viscosity coupling) gave significant changes in KRQA variables %REC, %DET, and LMAX (not shown). This example illustrates the ease with which cross-recurrence analysis handles non-linearities in short data sets, and at a higher resolution than the FFT to boot.

There is still much work to be done with respect to cross-recurrence analysis, but it is posited that KRQA may be a formidable tool in the examination of coupled oscillators. This may be particularly true for coupled biological oscillators where subtle, short scale changes in coupling may indicate (forecast) altered dynamics that may or may not be healthful for the examined system in part or even the entire organism as a whole. Shockley (Chapter 4) presents a psychological application of KRQA.

RECURRENCE PATTERNS OF SPEECH

Recurrence analysis, auto-recurrence or cross-recurrence, is fully amenable to linguistic systems or symbolic dynamics. Actually, one of the easiest explanations of recurrence can be purchased at the price of the simple children's book authored by Dr. Seuss (Geisel, 1960), *Green Eggs and Ham*. Webber and Zbilut (1996, 1998) have repeatedly used this example for instructive purposes. The reasoning goes as follows. Ask a child this riddle, "How can Dr. Seuss write a book with 812 words if he has a limited vocabulary of only 50 words?" The obvious answer is that words must be reused—that is, words recur. While we are at it, why not ask the child, "How can books with thousands of words be written in English, if there are only 26 alphabet letters available?" In this case, letters must be reused. So at the word

level or orthographic (spelling) level, symbols are simply reused in any combination desired by the author, as long as they correspond to allowable words in the language of choice. Common experience informs us that letters in words or words in sentences do not, and need not, appear at periodic intervals. Rather, actual linguistic sequences are at once highly nonlinear and highly meaningful as well. In this context, Orsucci, Walter, Giuliani, Webber, and Zbilut (1999) implemented RQA to study the linguistic structuring of American poems, Swedish poems, and Italian translations of the Swedish poems. They found invariance among the various language exemplars, suggesting hidden structuring at the orthographic level.

It is intriguing to consider the potential ability of recurrence strategies in the analysis of written text or spoken words as first explored by Orsucci et al. (1999) using American and Italian speech samples. Do different authors or various speakers have specific recurrence signatures that betray their individual identities? We might proceed at the orthographic level, rendering any speech text numeric by arbitrarily substituting integers for letters: A=1; B=2; C=3;...; X=24; y=25; Z=26; and for numbers: 0=27; 1=28; 2=29 ...; 7=34; 8=35; 9=36. We can keep things simple by ignoring cases of letters, all punctuation marks, spaces, carriage returns, and linefeeds. But how should the recurrence parameters be set? Well, since the encoding scheme is entirely arbitrary (we could have used: Z=1; Y=2; X=3; ...; etc.), the most important constraint is that the radius must be set to 0 distance units. This will insure that only identical letters (unique integers) will recur with each other. The embedding dimension can be set to one or higher, but for M > 1 the delay should be set to one so as not to skip any

letters in the string. The length of the text sets the maximum size of the window, but smaller windows can parcel the text into a series of epochs. It makes no difference whether the distance matrix is rescaled or not, because the only allowable radius is 0 units. The line parameter should be set to 2, lest one wants to exclude short words longer than two characters each (but that is not advised). With these preliminaries complete, what might diagonal line structures in the recurrence plot signify? If only identical letters count as recurrent points, a string of diagonal recurrences must indicate that the identical string of characters appears at different positions in the text. Actually, lines of varying length must represent words of varying length. Very loosely speaking, we might (correctly) envisage words as vectors of letters! In any case, recurrence quantifications can be captured in the seven recurrence variables we have discussed at length with respect to other dynamical systems.

But let us leave the letter level, and focus rather on words. We now face a new problem, one that involves choosing a scheme for encoding words. Unlike English letters that are limited to 26 characters and 10 digits, English words can number in the hundreds of thousands. For example, The Oxford English Dictionary Online (2003) has some 290,000 entries and 616,500 different English word forms. To encode words, we can assign ascending integer values to each new word, but whenever a former word recurs, its old integer value must be reused. To keep it simple, we can treat all punctuation marks as spaces. After the full text is encoded, the total number of integers in the derived file must equal the total number of words in the text. The number of

different words in the text (vocabulary size) will be represented by the numerical value of the largest integer.

It has long been known that the psychiatric illness of schizophrenia is characterized by disordered speech (Kasanin & Lewis, 1944). So to provide a practical example of quantitative textual analysis using RQA strategies, let us examine the speech patterns of a schizophrenic patient and "normal" academic as quoted by Wróbel (1990). Each quote consists of exactly 165 words. First quoted is the schizophrenic (Wróbel, 1990, p. 77), the context of which reveals this patient's altered sense of reality. To get the gist of how the 165 words were encoded, here are the codes for the first 26 words ("pre-started" counts as 2 words due to replacement of the dash with a space): 1-2-3-4-5-6-7-8-9-10-11-12-13-*14-15-16*-17-18-*14-15-16*-3-19-18-14-20 (note the repeat pattern of *14-15-16*: "before me and"):

> In Wroclaw I pre-started to pray, you know, the psychiatrist Kobohen came before me and he stood before me and I also stood before him, because he came to the ward on a visit, you know, he came before and he says: oh, that's the new one—he says—he arrived today—he says and he made a sign of the cross, you know, like this before me. I felt in the presence of that such terrible desires to pray because of that cross, that I began praying incredibly, I prostrated myself, I prayed on my knees, prostrate, I so implored the Lord God as much as possible, you know, and I felt myself a ruler, you know, I thought I was the supreme ruler on this earth, that over the whole world I was the supreme ruler, I began praying so incredibly with various crosses, yes I prayed so incredibly with crosses, with perfection and in different ways. He was dismissed from there, …

Second quoted is a normal academic (Wróbel, 1990, p. 99) who speaks logically and with intent purpose. The first 26 words (of 165 words) were encoded as follows: 1-2-3-4-5-6-7-8-*9-10*-11-*9-10*-12-13-14-15-6-16-17-18-19-20-21-22-23 (note the repeat pattern of *9-10*: "of the").

> Newtonian mechanics, for example, imposes a unified form of the description of the world. Let us imagine a white surface with irregular black spots on it. We then say that whatever kind of picture these make, I shall be able to approximate as closely as I wish to the description of it by covering the surface with a sufficiently fine square mesh, and saying of every square whether it is black or white. In this way I shall have imposed a unified form on the description of surface. The form is optional, since I could have achieved the same result by using a net with a triangular or hexagonal mesh. Possibly the use of a triangular mesh would have made the description simpler: that is to say, it might be that we could describe the surface more accurately with a coarse triangular mesh than with a fine square mesh (or conversely), and so on. The different nets correspond to different systems for describing the world.

Recurrence plots were constructed for the 165 words of text comprising each subject's speech as shown in Figure 2.17. Here, M = 1, DELAY = 1, and RADIUS = 0. The "time series" beside each recurrence plot present as "saw-tooth" patterns due to the reusing (recurrence) of words. Recurrent points are plotted only when exact word matches are found. Recurrence quantifications are reported in Table 2.1 for these two subjects, both at the orthographic and word levels, before and after random shuffling. The 742-character normal text was truncated to 670 characters to match the number of characters

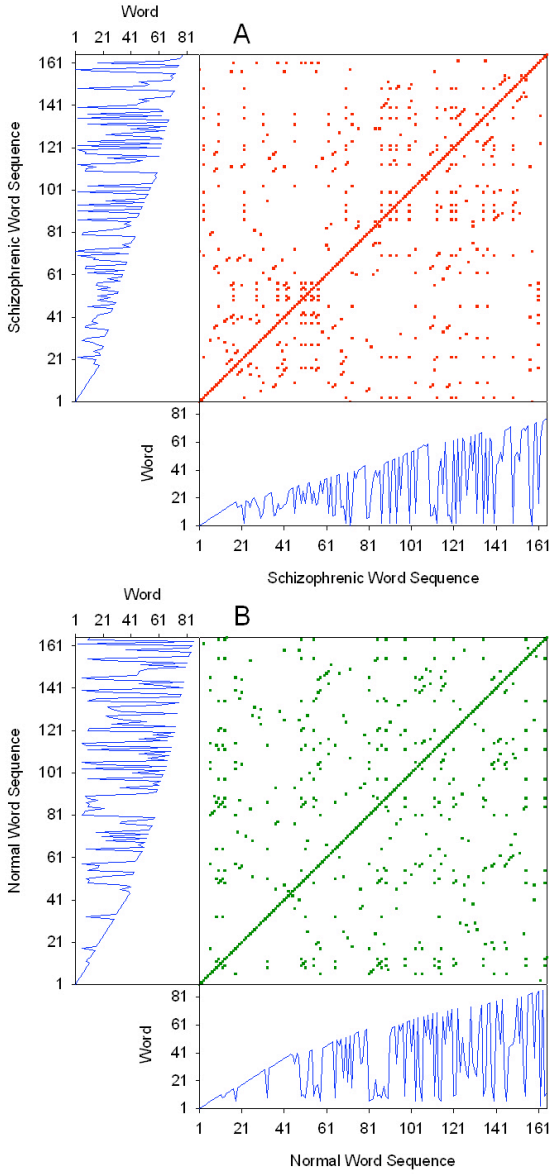

Figure 2.17. Recurrence analysis of human speech patterns at the word level. (A) Schizophrenic speech. (B) Normal speech. Recurrences occur only for exact word matches. Recurrence data computed from individual files *SCHIZWRD* and *NORMWRD* using program *RQD.EXE*. RQA parameters: P_1-P_{last} = 1-165; RANDSEQ = n; NORM = Euclid; DELAY = 1; EMBED = 1; RESCALE = absolute; RADUS = 0; COLORBND = 1; LINE = 2. RQA variables for schizophrenic speech (A): %REC = 1.870; %DET = 26.087; LMAX = 5; ENT = 0.675; TND = –8.361; %LAM = 0.000; TT = undefined. RQA variables for normal speech (B): %REC = 1.567; %DET = 23.113; LMAX = 3; ENT = 0.773; TND = –1.898; %LAM = 0.000; TT = undefined. See also Table 1.

in the schizophrenic text. Cursory review of the data reveal more differences at the word level than orthographic level. Shuffling decidedly distorts the deterministic structures. Admittedly, these examples are only anecdotal exercises without statistical merit. But what is being emphasized is the potential for nonlinear recurrence methodology to be employed on different speech patterns from many subjects, with careful attention being paid to proper experimental design.

Table 2.1. *Recurrence quantification analysis of human speech patterns. Data were computed from native sequences (and shuffled sequences) of letters (data files* SCHIZLET *and* NORMLET*) and words (data files* SCHIZWRD *and* NORMWRD*) using program RQD.EXE.*

RQA Variable	**Schizophrenic Letters** (N = 670)	**Normal Letters** (N = 670)	**Schizophrenic Words** (N = 165)	**Normal Words** (N = 165)
%REC	6.511% (6.511%)	6.312% (6.312%)	1.870% (1.870%)	1.567% (1.567%)
%DET	22.257% (12.019%)	22.280% (11.600%)	26.087% (3.953%)	23.113% (0.943%)
LMAX	19 (4)	16 (4)	5 (2)	3 (2)
ENT	0.995 (0.317)	0.986 (0.359)	0.675 (0.000)	0.773 (0.773)
TND	0.104 (0.029)	0.251 (0.240)	–8.361 (2.108)	–1.898 (-1.898)
%LAM	4.495% (12.636%)	1.484% (18.576%)	0.000% (11.067%)	0.000% (0.943%)
TT	2.000 (2.185)	2.000 (2.104)	2.000 (undefined)	undefined (2.000)

RECURRENCE PATTERNS OF PROTEINS

It is a simple matter to move from recurrence analysis of English texts to amino acid patterns of proteins. The amino acid alphabet is a 20-letter code of naturally occurring amino acids found in eukaryotic proteins. Protein function depends upon protein shape in 3-dimensional space (tertiary and quartenary structures), and protein shape depends upon the specific 1-dimensional amino acid sequence. Thus, recurrence analysis of amino acid sequences may yield interesting differences among the various classes of proteins. One approach would be to encode amino acids with unique integers from 1 to 20 and perform RQA computations using M = 1, DELAY = 1, and RADIUS = 0. When this is done, however, it has been shown that amino acid sequences are only slightly different from shuffled sequences (Webber & Zbilut, 1998). That is, naturally occurring sequences are almost random sequences, at least in terms of arbitrary amino acid names (residues). But even at this lowly name level, cross recurrence plots may prove useful in identifying stretches of identical residue patches (e.g., between protein isoforms) which would graphically plot as long diagonal lines (identical matches) with intervening gaps (mis-matches).

A change in perspective is in order. Thinking through the problem, it becomes clear that what imparts a 3-dimensional shape to proteins is the physical properties of their 1-dimensional string of amino acids. Specific sequences of amino acids twist and fold on themselves, forming protein globules with specific features. Two of the strongest physical properties that amino possess are their hydrophobicity and net charge. By merely substituting the name of

each amino acid by one of its physical properties, it is possible to generate new sequence amenable for recurrence analysis in higher dimensions.

To illustrate, consider human hemoglobin, a quartenary protein with two alpha-chains (141 amino acids each) and two beta-chains (146 amino acids each) of amino acids. Recurrence quantifications were performed on the alpha chain, first at the orthographic level (M = 1; DELAY = 1; RADIUS = 0% maximum distance), and second following hydrophobic substitutions using the hydrophobicity scale of Miyazawa and Jernigan (1996) (M = 3; DELAY = 1; RADIUS = 5% maximum distance). Recurrence plots for both representations of the same system are shown in Figure 2.18. Recurrences seem denser for the hemoglobin residue names (orthographic level) then for their hydrophobic substitutions. Conversely, the diagonal line structuring seems to be more common in hydrophobic space. But we cannot trust our eyes, which always see things from our own biased perspective. Nevertheless, these first impressions are confirmed in the data of Table 2.2, which lists the results of RQA performed on native residue sequences as well as their randomly shuffled versions. Thus the hydrophobic representation of hemoglobin has a lower %REC but higher %DET than at the residue name ("spelling") level. The hydrophobic signal is also more complex (higher ENT value), a reflection of its greater non-stationarity (higher absolute TND value). The bottom line is that by transforming single-letter amino acid residues into hydrophobic signals, the amino-acid sequence can be

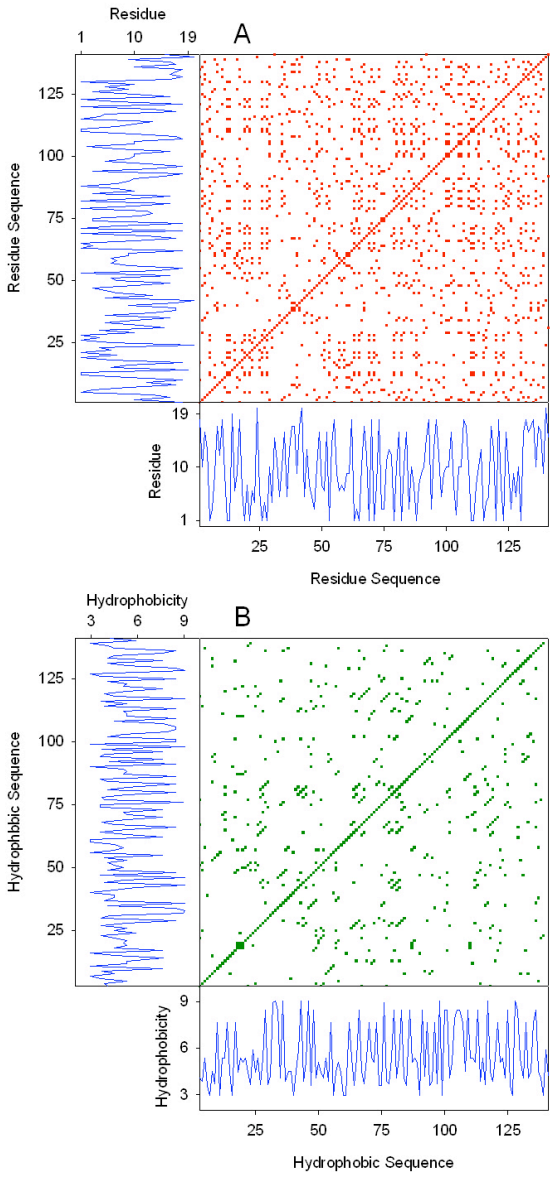

Figure 2.18. Recurrence analysis of human hemoglobin protein (alpha chain) at two levels. (A) Residue name level. Recurrences occur only for identical residue matches. Recurrence data computed from file *HEMOALET* using program *RQD.EXE*. RQA parameters: P_1-P_{last} = 1-139; RANDSEQ = n; NORM = Euclid; DELAY = 1; EMBED = 1; RESCALE = absolute; RADUS = 0; COLORBND = 1; LINE = 2. RQA variables: %REC = 7.518; %DET = 15.633; LMAX = 3; ENT = 0.219; TND = –2.002; %LAM = 12.129; TT = 2.000. (B) Residue hydrophobicity level. Recurrences occur for similar hydrophobic patches. Recurrence data computed from file *HEMOAHYD* using program *RQD.EXE*. RQA parameters: P_1-P_{last} = 1-139; RANDSEQ = n; NORM = Euclid; DELAY = 1; EMBED = 3; RESCALE = max dist; RADUS = 10; COLORBND = 1; LINE = 2. RQA variables: %REC = 2.669; %DET = 46.875; LMAX = 5; ENT = 1.113; TND = –6.289; %LAM = 0.781; TT = 2.000. See also Table 2.

projected into higher dimensional space (M > 1) where approximate recurrences become legitimate (RADIUS > 0). For these and other reasons RQA is making significant headway into the problem of protein folding (Zbilut, Sirabella, Giuliani, Manetti, Colosimo, & Webber, 2002; Giuliani, Benigni, Zbilut, Webber, & Sirabella, 2002).

Table 2.2. *Recurrence quantification analysis of human hemoglobin protein. Data were computed from native sequences (and shuffled sequences) of protein letters (data file* HEMOALET*) and protein hydrophobicities (data file* HEMOAHYD*) using program* RQD.EXE*.*

RQA Variable	**Hemoglobin-A Residue Names** (N = 141)	**Hemoglobin-A Hydrophobicity** (N = 141)
%REC	7.518% (7.518%)	2.669% (2.627%)
%DET	15.633% (10.377%)	46.875% (41.667%)
LMAX	3 (3)	5 (4)
ENT	0.219 (0.176)	1.113 (0.957)
TND	-2.002 (-8.333)	-6.289 (-5.814)
%LAM	12.129% (11.860%)	0.781% (8.730%)
TT	2.000 (2.000)	2.000 (2.000)

SUMMARY

The focus on this chapter has been on the proper implementation strategies of RQA. We have not emphasized the large and growing recurrence literature amassed over the last decade. Most of this literature, exceeding 170 references, is accessible from the website of Marwan (2003b). But it is appropriate here to just list several of the fields impacted by nonlinear recurrence analysis over the last decade: Chaos science (Trulla, Giuliani, Zbilut, & Webber, 1996), respiration (Webber, 1991), heartbeat dynamics (Giuliani, Piccirillo, Marigliano, & Colosimo, 1998), blood pressure (Mestivier, Dabire, Safar, & Chau, 1998), otoacoustic emissions (Zimatore, Hatzopoulos, Giuliani, Martini, & Colosimo, 2002), muscle fatigue (Farina, Fattorini, Felici, & Filligoi, 2002), postural control (Riley, Balasubramaniam, & Turvey, 1999), genomics (Bultrini, Pizzi, Del Giudice, & Frontali, 2003), proteomics (Zbilut et al., 2002), molecular dynamics (Manetti, Ceruso, Giuliani, Webber, & Zbilut, 1999), and even finance (Antoniou & Vorlow, 2000). In fact, any time series (or spatial series, for that matter) is amenable to RQA. If it wiggles in time (physiology) or space (anatomy) RQA can quantify the dynamic.

For parting thoughts, the mere fact that ants can lift 50 times their body weight whereas humans cannot is one lowly illustration of non-linearity in our shared world with insects. As we have seen, many of the dynamical, real-world systems common to man are notoriously non-linear, non-stationary, and noisy. To successfully analyze such systems it seems best to use non-linear tools that are independent of prescribed statistical distributions of the data (e.g., Gaussian), can deal with short data sets (e.g., polypeptides), are not stymied by actual signal

transients and outliers (e.g., observations beyond a few standard deviations of the mean), and can project the input signal into higher-dimensional space (e.g., embedding capabilities). So far, recurrence analysis seems to fit the bill in all of these important aspects. But the recurrence approach is not a stand-alone technique, some kind of end-all, be-all of extant nonlinear dynamical tools. For instance, significant advances are also being made by combining recurrence quantification analysis (RQA) with principle component analysis (PCA). By this means the complex relationship among the several recurrence variables can be objectively compared and processed as an ensemble (Zbilut, Giuliani, & Webber, 1998b; Giuliani, Colafranceschi, Webber, & Zbilut, 2001).

RQA functions like a microscope, snooping out higher-dimensional subtleties in the dynamics that are not obvious its first-dimensional representation. Returning to the animal world, one analogy would be with farmers who can best forecast weather patterns by observing altered behaviors of their barnyard livestock. Evidently, these domesticated animals can sense actual physical phenomena beyond the human sensory range. Indeed, Marino and Frilot (2003) used RQA strategies to convincingly demonstrate the sensitivity of rabbits to magnetic fields. In addition, Mohr, Langbein, and Nürnberg (2002) applied RQA to assess stress levels in calves and cows. But whatever the case, whether it be forecasting dynamical events in the medical field, geophysics, or meteorology, the future of recurrence analysis looks bright and promising.

SOFTWARE

Some investigators are writing their own programs to perform recurrence quantifications. But for those wishing to download recurrence software from the World Wide Web, at least three sites are available as shown below: *Visual Recurrence Analysis* (*VRA*) from Eugene Kononov; *Cross Recurrence Plots-Toolbox* (*CRP*) from Norbert Marwan; *RQA* (*Recurrence Quantification Analysis*) from Charles Webber.

VRA 4.6: http://home.netcom.com/~eugenek/download.html

CRP 4.5: http://www.agnld.uni-potsdam.de/~marwan/intro.html

RQA 8.1: http://homepages.luc.edu/~cwebber

REFERENCES

Antoniou, A., & Vorlow, C. (2000). Recurrence plots and financial time series analysis. *Neural Network World, 10,* 131-145.

Bassingthwaighte, J. B., Liebovitch, L. S., & West, B. J. (1994). *Fractal physiology.* New York: Oxford University Press.

Bultrini, E., Pizzi, E., Del Giudice, P., & Frontali, C. (2003). Pentamer vocabularies characterizing introns and intron-like intergenic tracts from Caenorhabditis elegans and Drosophila melanogaster. *Gene, 304,* 183-192.

Eckmann, J.-P., Kamphorst, S. O., & Ruelle, D. (1987). Recurrence plots of dynamical systems. *Europhysics Letters, 4,* 973-977.

Farina, D., Fattorini, L., Felici, F., & Filligoi G. (2002). Nonlinear surface EMG analysis to detect changes of motor unit conduction velocity and synchronization. *Journal of Applied Physiology, 93,* 1753-1763.

Feller, W. (1950). *An introduction to probability theory and its applications, Vol. 1*. New York: John Wiley & Sons.

Fraser, A. M., & Swiney, H. L. (1986). Independent coordinates for strange attractors from mutual information. *Physical Review A, 33,* 1134-1140.

Geisel, T.S. (Dr. Seuss, pseudonym) (1960). *Green eggs and ham.* New York: Random House, Inc.

Girault, P. (1991). Attractors and dimensions. In G. Cherbit (Ed.), *Fractals: Non-Integral Dimensions and Applications* (pp. 60-82). Chinchester: John Wiley & Sons.

Giuliani, A., Benigni, R., Zbilut, J. P., Webber, C. L., Jr., Sirabella, P., & Colosimo, A. (2002). Nonlinear signal analysis methods in the elucidation of protein sequence-structure relationships. *Chemical Reviews, 102*, 1471-1491.

Giuliani, A., Colafranceschi, M., Webber, C. L., Jr., & Zbilut, J. P. (2001). A complexity score derived from principal components analysis of nonlinear order measures. *Physica A,* 301, 567-588.

Giuliani, A., Piccirillo, G., Marigliano, V., & Colosimo, A. (1998). A nonlinear explanation of aging-induced changes in heartbeat dynamics. *American Journal of Physiology, 275,* H1455-H1461.

Glass, L., & Mackey, M.C. (1988). *From clocks to chaos: The rhythms of life.* Princeton: Princeton University Press.

Grafakos, L. (2003). *Classical and modern Fourier analysis.* Upper Saddle River: Prentice Hall.

Grassberger, P., & Procaccia, I. (1983). Measuring the strangeness of strange attractors. *Physica D, 9,* 189-208.

Grassberger, P., Schreiber, T., & Schaffrath, C. (1991). Non-linear time series analysis. *International Journal of Bifurcation and Chaos, 1,* 521-547.

Hénon, M. (1976). A two-dimensional mapping with a strange attractor. *Communications in Mathematical Physics, 50,* 69-77.

Kac, M. (1959). *Probability and related topics in physical sciences.* New York: Interscience Publishers.

Kaplan, D., & Glass, L. (1995). *Understanding nonlinear dynamics.* New York: Springer Verlag.

Kasanin, J. S., & Lewis, N. D. C. (1944). *Language and thought in schizophrenia: Collected papers.* Berkeley: University of California Press.

Kennel, M. B., Brown, B., & Abarbanel, H. D. I. (1992). Determining embedding dimension for phase-space reconstruction using a geometrical construction. *Physical Review A, 45,* 3403-3411.

Lorenz, E. N. (1963). Deterministic non-periodic flows. *Journal of Atmospheric Sciences, 20,* 130-141.

Manetti, C., Ceruso, M.-A., Giuliani, A., Webber, C. L., Jr., & Zbilut, J. P. (1999). Recurrence quantification analysis as a tool for the characterization of molecular dynamics simulations. *Physical Review E, 59,* 992-998.

Marino, A. A., & Frilot, C. (2003). Localization of electroreceptive function in rabbits. *Physiology and Behavior, 79,* 803-810.

Marwan, N. (2003a). *Encounters with neighbors: Current developments of concepts based on recurrence plots and their application.* Unpublished doctoral dissertation, Institute for Physics, University of Potsdam.

Marwan, N. (2003b). Cross recurrence plots toolbox. http://www.agnld.uni-potsdam.de/~marwan/intro.html

Marwan, N., Wessel, N., Meyerfeldt, U., Schirdewan, A., & Kurths, J. (2002). Recurrence-plot-based measures of complexity and their application to heart rate variability data. *Physical Review E, 66,* 026702.1-026702.8.

Mayer-Kress, G., & Holzfuss, J. (1987). Analysis of the human electroencephalogram with methods from nonlinear dynamics. In L. Rensing, U. van der Heiden, & M. C. Mackey (Eds.), *Temporal Disorder in Human Oscillatory Systems* (pp. 57-68). Berlin: Springer-Verlag.

Mestivier, D., Dabire, H., Safar, M., & Chau, N. P. (1998). Use of nonlinear methods to assess effects of clonidine on blood pressure in spontaneously hypertensive rats. *Journal of Applied Physiology, 84*, 1795-1800.

Misulis, K. E., & Head, T. C. (2003). *Essentials of clinical neurophysiology* (3rd edition). Burlington: Butterworth-Heinemann.

Miyazawa, S., & Jernigan, R. L. (1996). Residue-residue potentials with a favorable contact pair term and an unfavorable high packing density term, for simulation and threading. *Journal of Molecular Biology, 256,* 623-644.

Mohr, E., Langbein, J., & Nürnberg, G. (2002). A noninvasive approach to measure stress in calves and cows. *Physiology and Behavior, 75,* 251-259.

Orsucci, F., Walter, K., Giuliani, A., Webber, C. L., Jr., & Zbilut, J. P. (1999). Orthographic structuring of human speech and texts: Linguistic application of recurrence quantification analysis. *International Journal of Chaos Theory Applications, 4,* 21-28.

The Oxford English Dictionary Online, (2003). http://www.oed.com Oxford: Oxford University Press.

Parker , T. S, & Chua, L. O. (1989). *Practical numerical algorithms for chaotic systems.* New York: Springer-Verlag.

Riley, M. A., Balasubramaniam, R., & Turvey, M. T. (1999). Recurrence quantification analysis of postural fluctuations. *Gait and Posture, 9,* 65-78.

Shannon, C. E. (1948). A mathematical theory of communication. *Bell Systems Technical Journal, 27*, 379-423 & 623-656.

Shockley, K., Buttwill, M., Zbilut, J. P., & Webber, C. L., Jr. (2002). Cross recurrence quantification of coupled oscillators. *Physics Letters A, 305,* 59-69.

Takens, F. (1981). Detecting strange attractors in turbulence. In D. Rand, & L.-S. Young (Eds.), *Lecture Notes in Mathematics, Vol. 898, Dynamical Systems and Turbulence, Warwick 1980* (pp. 366-381). Berlin: Springer-Verlag.

Thomasson, N., Hoeppner, T. J., Webber, C. L., Jr., & Zbilut, J. P. (2001). Recurrence quantification in epileptic EEGs. *Physics Letters A, 279,* 94-101.

Thomasson, N., Webber, C. L., Jr., & Zbilut, J. P. (2002). Application of recurrence quantification analysis to EEG signals. *International Journal of Computer Applications, 9,* 1-6.

Trulla, L. L., Giuliani, A., Zbilut, J. P., & Webber, C. L., Jr. (1996). Recurrence quantification analysis of the logistic equation with transients. *Physics Letters A, 223,* 255-260.

Webber, C. L., Jr. (1991). Rhythmogenesis of deterministic breathing patterns. In H. Haken & H. P. Koepchen (Eds.), *Rhythms in Physiological Systems* (pp. 177-191). Berlin, Heidelberg, New York: Springer-Verlag.

Webber, C. L., Jr. (2004). Introduction to recurrence quantification analysis. *RQA version 8.1 README.TXT:* http://homepages.luc.edu/~cwebber/

Webber, C. L., Jr., Schmidt, M. A., & Walsh, J. M. (1995). Influence of isometric loading on biceps EMG dynamics as assessed by linear and nonlinear tools. *Journal of Applied Physiology, 78,* 814-822.

Webber, C. L., Jr., & Zbilut, J. P. (1994). Dynamical assessment of physiological systems and states using recurrence plot strategies. *Journal of Applied Physiology, 76,* 965-973.

Webber, C. L., Jr., & Zbilut, J. P. (1996). Assessing deterministic structures in physiological systems using recurrence plot strategies. In M. C. K. Khoo (Ed.), *Bioengineering Approaches to Pulmonary Physiology and Medicine* (pp. 137-148). New York: Plenum Press.

Webber, C. L., Jr., & Zbilut, J. P. (1998). Recurrent structuring of dynamical and spatial systems. In A. Colosimo (Ed.) *Complexity in the Living: A Modelistic Approach* (pp. 101-133). Proceedings of an International Meeting, February 1997, University of Rome "La Sapienza."

Wróbel, J. (1990). *Language and schizophrenia.* Amsterdam: John Benjamins Publishing Company.

Wyner, A. D., Ziv, J., & Wyner, A. J (1998). On the role of pattern matching in information theory. *IEEE Transactions on Information Theory, 44,* 2045-2056.

Zbilut, J. P., Giuliani, A., & Webber, C. L., Jr. (1998a). Detecting deterministic signals in exceptionally noisy environments using cross-recurrence quantification. *Physics Letters A, 246,* 122-128.

Zbilut, J. P., Giuliani, A., & Webber, C. L., Jr. (1998b). Recurrence quantification analysis and principle components in the detection of short complex signals. *Physics Letters A, 237,* 131-135.

Zbilut, J. P., Sirabella, P., Giuliani, A., Manetti, C., Colosimo, A., & Webber, C. L., Jr. (2002). Review of nonlinear analysis of proteins through recurrence quantification. *Cell Biochemistry and Biophysics, 36,* 67-87.

Zbilut, J. P., & Webber, C. L., Jr. (1992). Embeddings and delays as derived from quantification of recurrence plots. *Physics Letters A, 171,* 199-203.

Zimatore, G., Hatzopoulos, S., Giuliani, A., Martini, A., & Colosimo, A. (2002). Comparison of transient otoacoustic emission responses from neonatal and adult ears. *Journal of Applied Physiology, 92,* 2521-2528.

APPENDIX: Mathematical Construction of the Recurrence Matrix

(Webber, 2004)

RQA employs the method of time delays to embed experimental data into higher dimensions. Explicit examples of how distance matrices (DM) and recurrence matrices (RM) are constructed for Euclidean, maximum, and minimum norms are detailed below for a contrived time-series vector (TS) with 29 elements.

TS = [3.7, 9.2, 2.1, –5.4, 0.0, –10.9, 9.2, 3.1, 1.7, 1.8, –0.3, –4.9, 2.7, 3.5, 7.5, –9.9, –9.9, –4.7, 1.3, 2.7, 7.6, 3.9, 7.3, 8.0, 0.3, –1.9, 5.1, 8.8, 8.2]

For DELAY=8, EMBED=4, FIRST=1 and LAST=5, the following 5 time-delay vectors are constructed:

V1 = [+3.7, +1.7, –9.9, +0.3]
V2 = [+9.2, +1.8, –4.7, –1.9]
V3 = [+2.1, –0.3, +1.3, +5.1]
V4 = [–5.4, –4.9, +2.7, +8.8]
V5 = [+0.0, +2.7, +7.6, +8.2].

Comparison of the 5 vectors constructs a single 5 × 5 recurrence matrix of distances for each of the 3 norm types. For example, the Euclidean distance between vectors V4 and V5 is calculated as follows:

DM(Euclid norm at i=4, j=5) = SQRT (SQR(–5.4 – 0.0)+(SQR(–4.9 – 2.7)+ SQR(2.7 – 7.6) + SQR(8.8 – 8.2)) = 10.549.

To compute the maximum and minimum distances between vectors V4 and V5, the vectors are compared element by element.

ABS(–5.4 – 0.0) = 5.4
ABS(–4.9 – 2.7) = 7.6 (largest difference)
ABS(2.7 – 7.6) = 4.9
ABS(8.8 – 8.2) = 0.6 (smallest difference)

By definition, maximum and minimum distances are simply the maximum and minimum differences, respectfully.

DM(max norm at i=4, j=5) = 7.6
DM(min norm at i=4, j=5) = 0.6

This procedure is repeated for each cell, giving the following results for DM(i,j). Only the distances in the upper triangle are shown since the lower half is perfectly symmetrical. Note that the central diagonal is designated by 0.00 distances (vector identity matches).

DM(Euclid norm) =
[1,5]=19.58; [2,5]=18.41; [3,5]=7.92; [4,5]=10.55; [5,5]=0.00
[1,4]=18.90; [2,4]=20.67; [3,4]=9.65; [4,4]=0.00
[1,3]=12.45; [2,3]=11.83; [3,3]=0.00
[1,2]=7.88; [2,2]=0.00
[1,1]=0.00

DM(max norm) =
[1,5]=17.50; [2,5]=12.30; [3,5]=6.30; [4,5]=7.60; [5,5]=0.00
[1,4]=12.60; [2,4]=14.60; [3,4]=7.50; [4,4]=0.00
[1,3]=11.20; [2,3]=7.10; [3,3]=0.00
[1,2]=5.50; [2,2]=0.00
[1,1]=0.00

DM(min norm) =
[1,5]=1.00; [2,5]=0.90; [3,5]=2.10; [4,5]=0.60; [5,5]=0.00
[1,4]=6.60; [2,4]=6.70; [3,4]=1.40; [4,4]=0.00
[1,3]=1.60; [2,3]=2.10; [3,3]=0.00
[1,2]=0.10; [2,2]=0.00
[1,1]=0.00

These distances are all expressed in absolute units and can be retained as such by selecting rescaling option 1.

By selecting rescaling option 2, RM distances are normalized to the mean distance of the RM by dividing each cell by the absolute mean distance and multiplying by 100. All central diagonal values of zero are excluded from the calculation of mean distance.

DM mean distance (Euclid norm) = 13.783 = 100.0%
DM mean distance (max norm) = 10.220 = 100.0%
DM mean distance (min norm) = 2.310 = 100.0%

By selecting rescaling option 3, DM distances are normalized to the maximum distance of the DM by dividing each cell by the absolute maximum distance and multiplying by 100. Be careful not to confuse max distance and max norm, which are different.

DM max distance (Euclid norm) = 20.671 = 100.0%
DM max distance (max norm) = 17.500 = 100.0%
DM max distance (min norm) = 6.700 = 100.0%

Recurrence matrices are derived from distance matrices by setting a RADIUS threshold. As shown below, the Heavyside function assigns values of 0 or 1 to array elements. The RADIUS parameter is always relative to the reported MAXDIST, whether it be expressed in absolute units or relative units. Only those distances in RM[I,J] equal to or less than the RADIUS are defined as recurrent points at coordinates I, J.

RM (Euclid norm with RADIUS of 8.0) =
[1,5]=0; [2,5]=0; [3,5]=1; [4,5]=0; [5,5]=1
[1,4]=0; [2,4]=0; [3,4]=0; [4,4]=1
[1,3]=0; [2,3]=0; [3,3]=1
[1,2]=1; [2,2]=1
[1,1]=1

RM (max norm with RADIUS of 12.3) =
[1,5]=0; [2,5]=1; [3,5]=1; [4,5]=1; [5,5]=1
[1,4]=0; [2,4]=0; [3,4]=1; [4,4]=1
[1,3]=1; [2,3]=1; [3,3]=1
[1,2]=1; [2,2]=1
[1,1]=1

RM (min norm with RADIUS of 1.2) =
[1,5]=1; [2,5]=1; [3,5]=0; [4,5]=1; [5,5]=1
[1,4]=0; [2,4]=0; [3,4]=0; [4,4]=1
[1,3]=0; [2,3]=0; [3,3]=1
[1,2]=1; [2,2]=1
[1,1]=1

RQA looks for patterns among these recurrent points, and this need not/must not be done manually (too subjective). Objective pattern recognition algorithms are written into the many recurrence programs to define the RQA variables %REC, %DET, ENT, LMAX, TND, %LAM, and TT.